©2007 Society of Economic Geologists, Inc.
Economic Geology, v. 102, pp. 1129–1155

Bald Mountain Gold Mining District, Nevada: A Jurassic Reduced Intrusion-Related Gold System

C. J. Nutt† and A. H. Hofstra

U.S. Geological Survey, Box 25046, Mail Stop 973, Denver Federal Center, Denver, Colorado 80209

Abstract

The Bald Mountain mining district has produced about 2 million ounces (Moz) of Au. Geologic mapping, field relationships, geochemical data, petrographic observations, fluid inclusion characteristics, and Pb, S, O, and H isotope data indicate that Au mineralization was associated with a reduced Jurassic intrusion. Gold deposits are localized within and surrounding a Jurassic (159 Ma) quartz monzonite porphyry pluton and dike complex that intrudes Cambrian to Mississippian carbonate and clastic rocks. The pluton, associated dikes, and Au mineralization were controlled by a crustal-scale northwest-trending structure named the Bida trend. Gold deposits are localized by fracture networks in the pluton and the contact metamorphic aureole, dike margins, high-angle faults, and certain strata or shale-limestone contacts in sedimentary rocks. Gold mineralization was accompanied by silicification and phyllic alteration, ±argillic alteration at shallow levels. Although Au is typically present throughout, the system exhibits a classic concentric geochemical zonation pattern with Mo, W, Bi, and Cu near the center, Ag, Pb, and Zn at intermediate distances, and As and Sb peripheral to the intrusion. Near the center of the system, micron-sized native Au occurs with base metal sulfides and sulfosalts. In peripheral deposits and in later stages of mineralization, Au is typically submicron in size and resides in pyrite or arsenopyrite. Electron microprobe and laser ablation ICP-MS analyses show that arsenopyrite, pyrite, and Bi sulfide minerals contain 10s to 1,000s of ppm Au. Ore-forming fluids were aqueous and carbonic at deep levels and episodically hypersaline at shallow levels due to boiling. The isotopic compositions of H and O in quartz and sericite and S and Pb in sulfides are indicative of magmatic ore fluids with sedimentary sulfur. Together, the evidence suggests that Au was introduced by reduced S-bearing magmatic fluids derived from a reduced intrusion. The reduced character of the intrusion was caused by assimilation of carbonaceous sedimentary rocks.

Tertiary faults dismember the area and drop down the upper part of the mineralizing system to the west. The abundant and widespread kaolinite in oxide ores is relatively disordered (1A polytype) and has δD and δ^{18}O values suggestive of a supergene origin. The deep weathering and oxidation of the ores associated with exhumation made them amenable to open-pit mining and processing using cyanide heap leach methods.

Introduction

Mineral deposits in Nevada account for about 70 percent of the Au produced in the United States. The majority of Au is mined from Carlin-type Au deposits in the Carlin, Battle Mountain-Eureka, Getchell, and Independence (Jerritt Canyon) trends (Fig. 1A; Hofstra and Cline, 2000; Cline et al., 2005). Most Carlin-type deposits are considered to have formed in the Tertiary (Henry and Boden, 1998; Hofstra et al., 1999; Ressel and Henry, 2006). Nevada also contains significant Tertiary epithermal Au-Ag deposits and Tertiary and Cretaceous porphyry-related base metal-Au deposits (John et al., 2003). Examples of Tertiary porphyry Cu-Au deposits (Fig. 1A) include the Battle Mountain district (Theodore, 2000) and the world-class Bingham deposit near Salt Lake City, Utah (Babcock et al., 1995, and references therein), which is located along a westerly mineral trend that extends into Nevada (Shawe, 1977). Less common and smaller Cretaceous Cu-Mo-Au deposits and related base metal-Au skarn and replacement deposits are present near the towns of Ely (Westra, 1979) and Eureka (Nolan, 1962; Fig. 1B). Distal disseminated Au deposits, with some features resembling Carlin-type Au deposits, are commonly associated with the Cretaceous and Tertiary porphyry systems.

Jurassic igneous rocks are typically associated with nil or minor Au concentrations and generally are not targets for exploration. In the eastern Great Basin, minor Au is associated with intrusive rock in the porphyry-related Cu deposit at the small Victoria mine in the Dolly Varden Mountains (Atkinson et al., 1982), replacement Ag, Pb, and Au deposits in the Cortez Range (Stewart and McKee, 1977), and base and precious metal skarn and polymetallic veins associated with the Goldstrike pluton in the northern Carlin trend (Emsbo et al., 2000; Heitt et al., 2003). In the western Great Basin, the Jurassic Yerington porphyry system has low Au (Dilles and Profett, 2000).

The Bald Mountain mining district is in east-central Nevada, about 115 km south-southeast of Elko and about 100 km northwest of Ely (Fig. 1B). The district contains 11 orebodies (Fig. 2) that cluster in and around the Bald Mountain pluton and are hosted by Cambrian to Jurassic rocks. In this paper, the deposits in Figure 2 are classified as follows: central and deep (Top, Mahoney, Sage Flat); peripheral and deep (LJ Ridge, LBM, Rat, 1–5 pits); central and shallow (RBM; acronyms are actual mine names). The deposits are enriched in base and precious metals and several trace elements (Table 1), particularly As, Sb, Zn, and Bi. Disseminated Au mineralization occurs along high-angle faults, in certain strata, and in stockworks and veins. In and near the Bald Mountain pluton, quartz stockworks and veins host ore at the Top, Mahoney, and Sage Flat deposits, whereas in the peripheral Rat and LJ Ridge deposits, ore is both discordant and concordant to bedding.

† Corresponding author: email, cnutt@usgs.gov

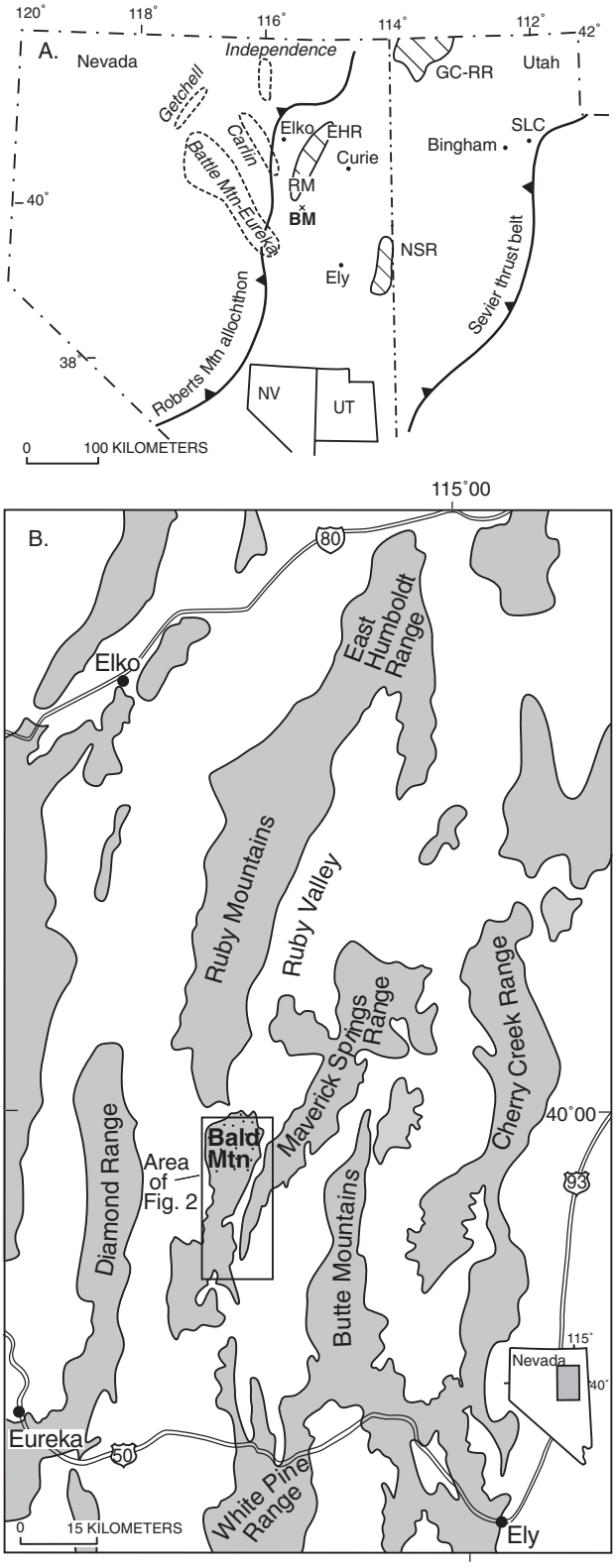

FIG. 1. Index maps showing (A) the location of the Bald Mountain mining district and important features in the eastern Great Basin. Gold trends outlined by dashes, core complexes denoted by diagonal lines. BM = Bald Mountain, EHR = East Humboldt Range, GC-RR = Grouse Creek-Raft River Mountains, NSR = northern Snake Range, RM = Ruby Mountains, SLC = Salt Lake City and (B) detail of the Bald Mountain area and nearby ranges.

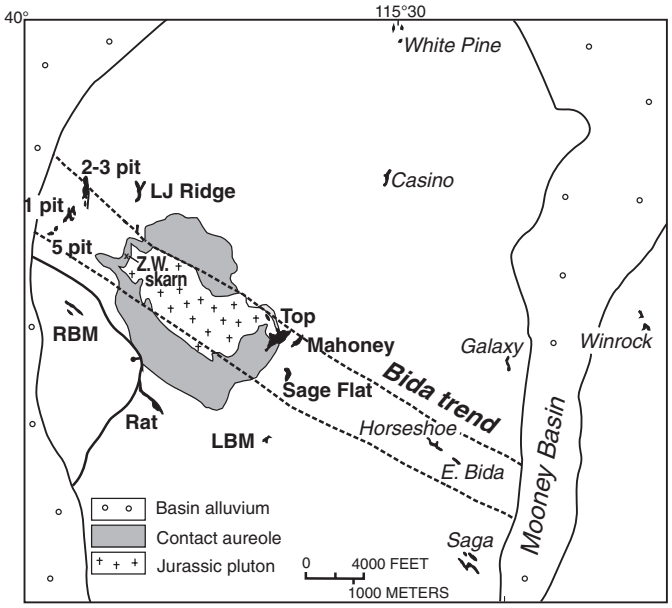

FIG. 2. Gold deposits in the Bald Mountain area. Deposits in bold are considered Jurassic deposits related to the Bald Mountain intrusion. Tertiary Mooney Basin Carlin-type deposits are labeled in italics as shown in Nutt and Hofstra (2003). Z.W. skarn = Jurassic Zed Williams skarn.

In 2006, Barrick Gold Corporation acquired the Bald Mountain, Mooney Basin, and Alligator Ridge-Yankee area properties (Fig. 3) and since then has been actively exploring and producing Au in the district. Deposits in the Bald Mountain area are hosted by Jurassic intrusive rock and Paleozoic sedimentary rocks and have produced about 2 million ounces (Moz) of Au from 11 orebodies in a 9- × 9-km area (Fig. 3; Nutt et al., 2000). The Bald Mountain district is on the southern extension of the Carlin trend (Fig. 1A) and west of the Alligator Ridge-Mooney Basin district (includes Yankee, Alligator Ridge, and all the deposits along Mooney Basin) interpreted to be Eocene in age and Carlin-type by Nutt and Hofstra (2003).

The north-trending Alligator Ridge-Mooney Basin district (Fig. 3) is controlled by a north-striking crustal structure (Rodriguez and Williams, 2001). These low-grade Carlin-type deposits are restricted to the upper part of the Devonian Guilmette Formation, the overlying Devonian to Mississippian Pilot Shale, and the lower part of the Mississippian Chainman Shale. The largest of the Mooney Basin deposits is at Alligator Ridge, where about 0.75 Moz of Au was recovered. Deep drilling through the deposit exposed no underlying intrusive rock, alteration, or mineralization. Other deposits, discovered to date along Mooney Basin are smaller than Alligator Ridge, typically <100,000 oz Au. These deposits have Carlin-type characteristics (i.e., Au is in arsenian pyrite rims on earlier pyrite; the geochemical signature is Au ± Sb ± As ± Hg; geologic reconstruction indicates that ore was deposited at shallow depths; fluid inclusions are small and difficult to find; jasperoid is abundant; realgar and orpiment are present (Nutt and Hofstra, 2003).

Our work in the Bald Mountain area is part of a mapping and deposit study that extends from the Alligator Ridge-Yankee area in the south to the Bald Mountain area to the north

TABLE 1. Downhole Geochemistry of the Bald Mountain Deposits (in ppm; modified from Nutt et al., 2000)

Deposit	Host	Hole no.	Feet	Au/Ag	Au	Ag	As	Sb	Hg	Tl	Cu	Pb	Zn	Mo	Bi	Te	Sn
RBM	Ji	RBM-240	270–290	0.27	6.14	22.7	1620	240	1.4	4.1	100	1030	19	42	250	na	na
Top/Mahoney/ Sage Flat	Op	RT-92	0–560	1.52	1.40	0.92	646	78	1.97	3.29	100	40	67	40	138	1.4	9.5
RBM	Mch									no	data						
Mahoney	Op/Cw	MCR-22	160–270	0.90	4.68	5.21	914	699	na	na	712	67	121	54	79	3.5	na
Sage Flat	Cw	RSC-11	480–630	1.96	2.37	1.21	940	559	na	na	593	24	146	115	238	3.7	na
Top, east side	Op/Cw	BDR-88	330–400	0.07	1.91	26.67	943	700	27.8	10.3	316	27	134	36	56	0.7	17
Top, skarn	Op/Cw/Cd	RT-41	250–290	18.17	4.18	0.23	1,332	161	8.8	40	42	6	55	45	215	0.8	23
LBM	Cw	85L-7	80–110	2.41	1.69	0.7	631	88	6.5	2.6	37	31	465	1.9	<1	<0.5	<20
LJ Ridge	Cd/Ch	LJR-052	340–380	9.75	7.80	0.8	1,696	1,343	<0.1	<0.1	28	102	125	4.8	<1	<0.1	<20
Rat (discordant)	Cd/Ch	RR-397	160–180	3.92	1.96	0.5	2,013	71	na	na	67	12	36	3.8	8.2	0.1	na
Rat (concordant)	Cd/Ch	RR-379	280–310	2.89	3.47	1.2	297	67	na	na	85	15	43	4.0	1.7	0.1	na
5 pit	Cd/Ch									no	data						
1 pit	Cg	R1-71	230–390	2.05	2.28	1.11	6,237	5,236	<0.1	0.8	39	46	395	1.3	1.0	<0.5	<1
2-3 pit	Cs	R3-100	230–340	1.00	3.65	3.66	2,346	9,066	<0.1	<0.5	38	23	659	4.8	0.18	<0.5	0.39
3 pit	Cs	R3-77	230–330	0.61	8.95	14.6	18,480	4,408	0.37	<0.5	120	299	2,662	8.3	0.87	<0.5	2.4

Abbreviations: Cd = Cambrian Dunderberg Shale, Cg = Cambrian Geddes Limestone, Ch =Cambrian Hamburg Limestone, Cw = Cambrian Windfall Formation, Ji = Jurassic pluton, Mch = Mississippian Chainman Shale, Op = Ordovician Pogonip Group

FIG. 3. Index map showing Bald Mountain and Alligator Ridge-Mooney Basin Au deposits. Bald Mountain deposits = squares, Alligator Ridge-Mooney Basin Carlin-type deposits (Nutt and Hofsta, 2003) = filled circles. Dotted line delineates Bida trend. Approximate area of Figures 2 and 4 are shown.

(Fig. 3). Detailed mapping of the area from south to north was previously reported in Nutt (2000) and Nutt and Hart (2004). Because the Bald Mountain district is adjacent to, and in part overlaps areas of Au mineralization along Mooney Basin, it was, and still is by some geologists, interpreted to be similar to the Carlin-type Alligator Ridge-Mooney Basin deposits. Hitchborn et al. (1996), however, proposed that most of the mineralization was related to a Jurassic intrusion. An early hypothesis was that Alligator Ridge-Mooney Basin mineralization had overprinted an earlier, small Jurassic mineralizing event that lacked appreciable Au. Instead, evidence described below and gathered from the mapping, age determinations, geochemistry, mineralogy, fluid inclusions, and isotopic studies of Nutt (2000), Nutt et al. (2000), Nutt and Hart (2004), and this study lead us to conclude that the Au deposits in the Bald Mountain district are products of a Jurassic reduced intrusion-related hydrothermal system and are distinct from the Eocene Carlin-type deposits in the Yankee-Alligator Ridge area. Reduced intrusion-related deposits are major producers of Au in interior Alaska, the Yukon, and elsewhere (McCoy et al., 1997; Thompson et al., 1999; Lang et al., 2000; Thompson and Newberry, 2000; Lang and Baker,

2001) but have previously not been recognized in the Great Basin.

Geologic Setting

The Bald Mountain mining district is primarily underlain by Proterozoic to Cambrian miogeoclinal clastic and carbonate rocks intruded by Jurassic and Tertiary igneous rocks and overlain by Tertiary sedimentary and volcanic rocks. Deformation has repeatedly affected the area. The Bald Mountain district is at the southern end of a crustal-scale feature that passes through the Carlin trend identified using Pb isotopes and interpreted by Tosdal et al. (2000) to be part of a Precambrian rift zone. The district is in the foreland of the Devonian-Mississippian Antler orogeny (Roberts Mountain allochthon) and the hinterland of the Mesozoic to early Tertiary Sevier thrust belt (Fig. 1A). The extent of Paleozoic structures is unknown but may reflect some movement along basement structures. East- to southeast-directed compression during the Sevier orogeny developed folds, reverse and thrust faults, and westerly trending strike-slip tear faults. That episode of contractional deformation was followed by Tertiary extension. At the southern end of the East Humboldt Range-Ruby Mountains core complex (EHR-RM, Fig. 1A), the Bald Mountain district is within a corridor of large magnitude Tertiary extension that includes the Northern Snake Range, East Humboldt Range-Ruby Mountain, and Raft River-Grouse Creek core complexes.

Cambrian through Mississippian carbonate and clastic rocks, a Jurassic pluton, and Eocene sedimentary and volcanic rocks crop out in the Bald Mountain area (Nutt and Hart, 2004). Both Jurassic intrusive and Paleozoic sedimentary rocks host Au ore. The oldest Paleozoic rocks, which are Cambrian and Ordovician in age, and Jurassic intrusive rocks, make up the central part of the Bald Mountain area. These rocks are bounded on the west by the Ruby normal fault and on the east by a series of down-to-the-east, north-northeast–striking normal faults (Fig. 4). The Paleozoic stratigraphic relationships and nomenclature are shown in Figure 5. The Cambrian rocks are calcareous shale (mostly carbonaceous and containing diagenetic pyrite), subordinate thin- to thick-bedded limestone, and, in the upper part, thick-bedded limestone. The Cambrian Bullwacker Member of the Windfall Formation contains karst breccias, best developed at the top of the unit, which hosts ore at the LBM and Sage Flat pits. In Cambrian rocks, ore is typically strata bound at and below the contact between limestone and overlying shale or thin-bedded limestone and discordant in shale-dominant lithologic units. Ordovician rocks are primarily thin-bedded silty limestone of the Pogonip Group, which can host ore, and the Eureka Quartzite. Above the Eureka Quartzite, there are 1,300 m of Silurian to Devonian dolomite that contain no ore. Dolomite is overlain by Devonian-Mississippian calcareous shale (commonly carbonaceous and containing diagenetic pyrite), limestone, and subordinate dolomite, and in the upper part, sandstone and conglomerate. The RBM mine occurs in the upper part of the Mississippian Chainman Shale. Details of the Paleozoic stratigraphy can be found in Blake (1964), Hose and Blake (1976), Hitchborn et al. (1996), Nutt (2000), Nutt et al. (2000), and Nutt and Hart (2004).

Eocene-Oligocene sedimentary and volcanic rocks are present in a downdropped block on the west side of the Ruby fault and along Mooney Basin. The rocks west of the Ruby fault are greatly disrupted, as described below, and are similar to Eocene rocks at Alligator Ridge (Nutt and Hofstra, 2003) that do not host ore. The sedimentary rocks are conglomerate, volcaniclastic sedimentary rock, and mudstone. A similar sequence at Alligator Ridge includes a lacustrine limestone dated as latest early to early middle Eocene age (~45 Ma) by identification of gastropods (Nutt and Good, 1998). Rhyolite flows, quartz-biotite tuff, and intermediate-composition flows are Eocene to early Oligocene. A rhyolite dike on the eastern side of Mooney Basin yielded a U-Pb age of 35.9 Ma (Mortenson et al. 2000).

A younger volcaniclastic unit with sandstone that contains clasts from the Eocene to Oligocene volcanic rocks crops out in Mooney Basin and in the Sage Flat pit, where it overlies altered and ore-bearing Ordovician rocks and contains a few pieces of reworked mineralized rock. This unit is Miocene or younger and indicates that the Sage Flat area, including the Top, Mohoney, and the Sage Flat ore deposits, was exposed and eroded during this time.

The dominant structural features in the area are (1) north- to northeast-striking faults; (2) a northwest-striking fault zone named the Bida trend (Figs. 2, 3), along which Jurassic igneous rock intruded; and (3) folds. Numerous episodes of faulting in the Bald Mountain area from the pre-Late Jurassic to Quaternary are expressed by faults that are intruded by Jurassic intrusive rock and subsequently displaced and by faults that cut Pleistocene fans along the western range front (Nutt and Hart, 2004).

North- to northeast-striking normal faults accommodated Tertiary extension and extend through the area, in some places for several kilometers. These faults displace orebodies in the area of the Top deposit. However, earlier movement on these faults also is indicated at the large Top orebody at the intersection of northeast- and northwest-striking faults (Fig. 4). In addition, on the deposit scale, ore throughout the Bald Mountain area is controlled, in part, by intersections of northeast and northwest faults and fractures (Hitchborn et. al, 1996). Jurassic dikes generally strike northwest and are only rarely present along the north- to northeast-striking faults.

The Bida trend is defined by a zone of northwest- to west-striking faults that are shorter and show smaller apparent displacements than north- to northeast-striking faults. The Bida trend is a major feature along which magma rose in the Jurassic. A magnetotelluric profile and interpretative geologic cross section across Bald Mountain indicate that the Bida trend is a near vertical, large crustal fault zone (Wannamaker and Doerner, 2002). Facies differences in the Cambrian Windfall Formation and the Ordovician Pogonip Group north and south of the trend may indicate that the zone of faults along the trend was active in the Paleozoic as well as in the Jurassic. The en echelon pattern of faults along the Bida trend (Nutt and Hart, 2004) now show normal offsets that displace Jurassic igneous rock and probably occurred by reactivation during Tertiary extension (Fig. 4). The ranges in northeastern and north-central Nevada are segmented by northeast- to southeast-striking tear, or strike-slip, faults associated with Mesozoic deformation, and the Bida trend may be one of these faults along which intrusions were emplaced in a pull-apart structure.

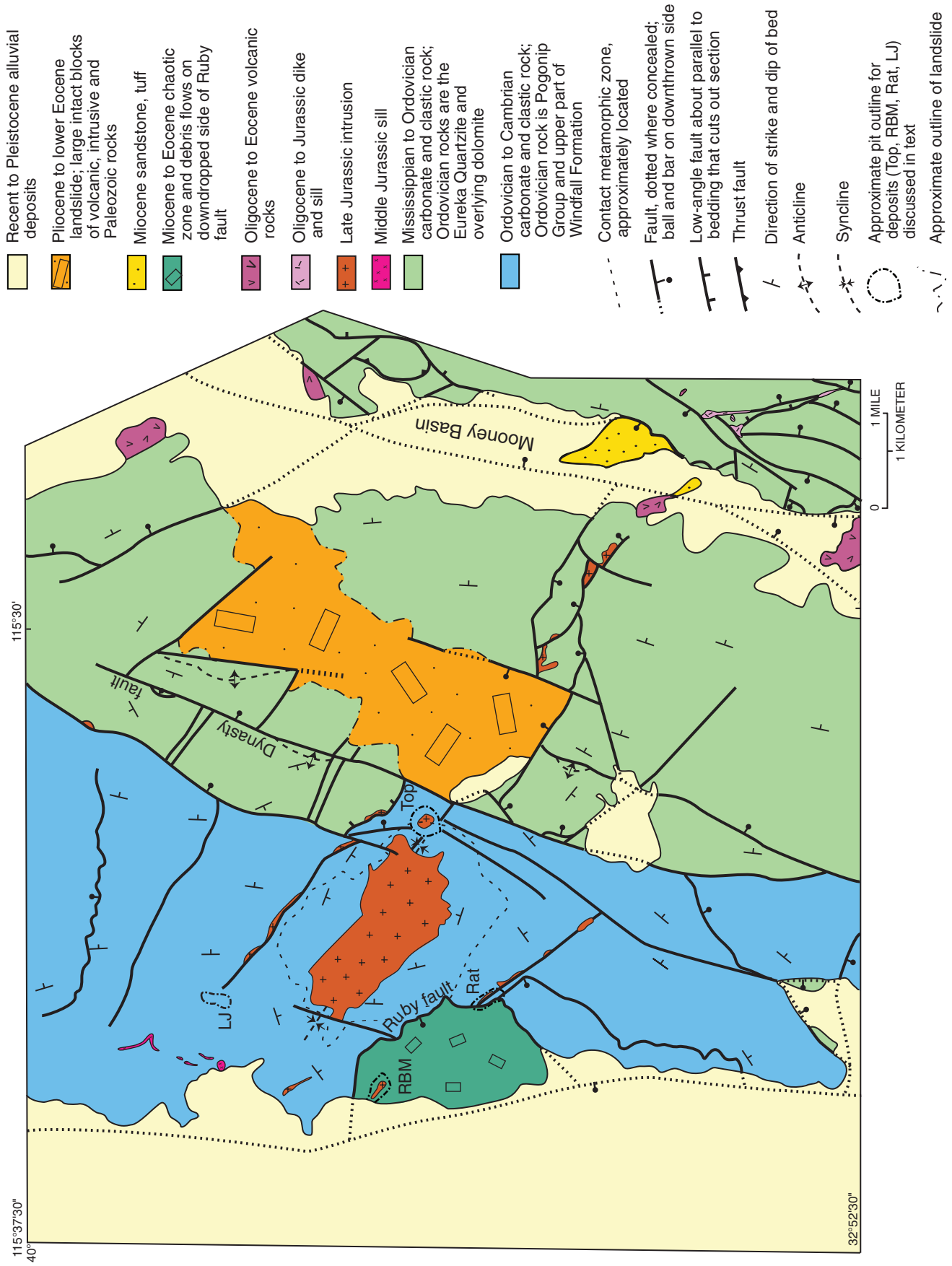

FIG. 4. Geologic map of the Bald Mountain area. See text for composition of igneous rocks. Modified from Nutt and Hart (2004).

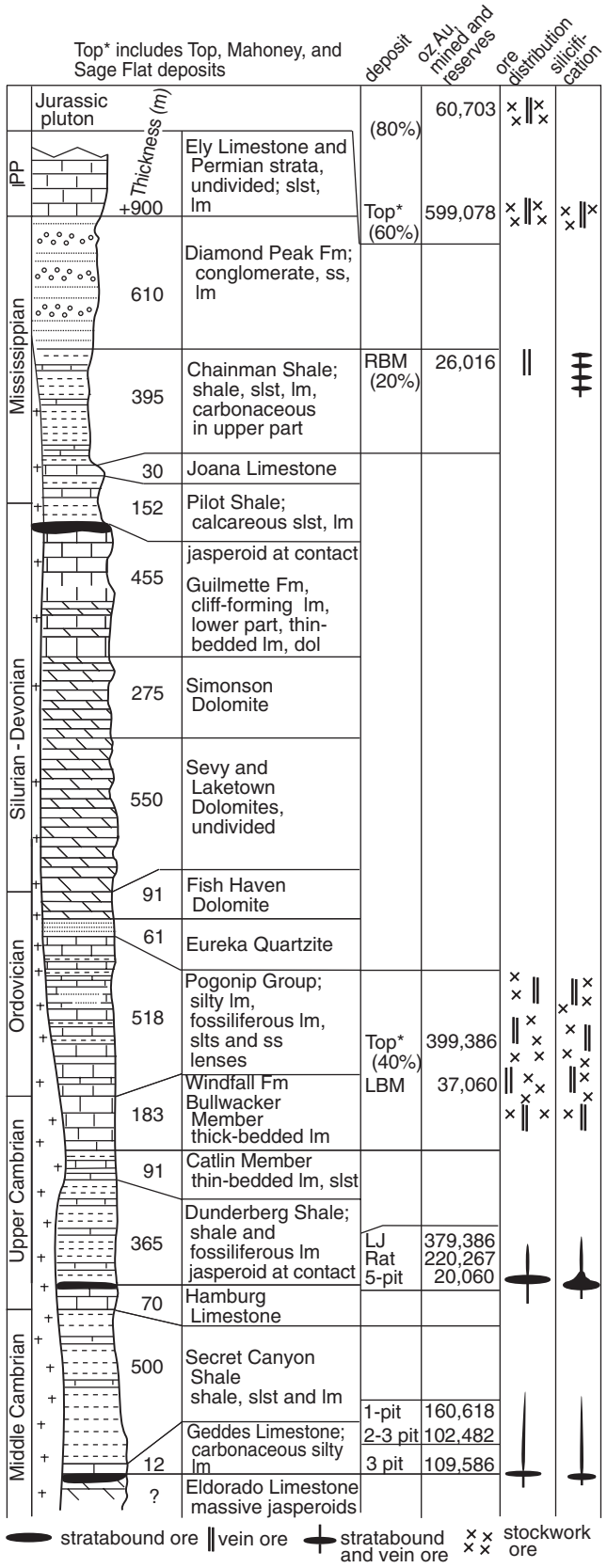

FIG. 5. Stratigraphic section of Bald Mountain area Paleozoic rocks, including Jurassic intrusive rock and host rocks for the deposits. Dol = dolomite, lm = limestone, slst = siltstone, ss = sandstone, Fm = formation.

The northerly Ruby fault (Figs. 4, 6) has the greatest amount of normal offset, which is as much as 2.8 km. In places, barren jasperoid occurs along the fault. The downdropped side is a chaotic zone that includes debris flows and blocks of Silurian to Mississippian rocks, 10s of meters up to a kilometer across, that are cut by Jurassic dikes and overlain by Eocene sedimentary and Eocene to Oligocene volcanic rocks. Offset on the Ruby fault is <35 Ma, which is the age of volcanic rocks that are part of the downdropped block (Nutt and Hart, 2004). The RBM deposit, which is hosted by Mississippian sedimentary rocks and the crosscutting Jurassic intrusion, occurs in one of the downdropped blocks (Fig. 4). The landslide on the east side of Big Bald Mountain is related to the northeast-striking Dynasty fault, which is one of the series of northeast-striking faults that drop down rocks to the east. The strata between the Dynasty and an eastern northeast-striking fault are locally displaced but mostly intact. The slide postdates mineralization, but its exact age is unknown. It includes Jurassic intrusive rock and Eocene to Oligocene volcanic rocks and is probably a Miocene-age feature.

Two types of folds are present: a northwest-trending syncline surrounding the Jurassic pluton, and a segmented north-trending anticline (Fig. 4). The north-trending anticline is similar to kilometer-long folds in the Alligator Ridge area (Nutt, 2000), but it is difficult to follow because it is cut by faults. In both the Alligator Ridge and Bald Mountain areas, north-trending folds are restricted to rocks younger than the Ordovician Eureka Quartzite, which suggests detachment along the Eureka Quartzite and disharmonic folding above the detachment. Evidence of this detachment surface includes north-trending folds that are constrained to the rocks above the Eureka Quartzite; underlying rocks dip consistently to the east.

Intrusive Rock

The Late Jurassic Bald Mountain pluton is a northwest-elongate coarse-grained quartz monzonite to granodiorite intrusion composed predominantly of potassium feldspar, quartz, plagioclase, and biotite (Fig. 4). Zircon from the pluton yielded a U-Pb age of 159.0 ± 0.5 Ma (Mortensen et al., 2000). No aeromagnetic anomaly is associated with the Bald Mountain intrusion (Ponce, 1991). An interpretive cross section based upon a magnetotelluric survey suggests that intrusive rock extends to a depth of up to 12 km (Wannamaker and Doerner, 2002). The pluton was emplaced into Cambrian and Ordovician sedimentary rocks, which were metamorphosed to skarn, hornfels, and/or marble for up to 1.5 km from the contact. The nature of the contact metamorphism depends on the original rock: Cambrian calcareous shales are metamorphosed to banded calcite-tremolite-quartz hornfels and limestones are metamorposed to marble with minor tremolite and quartz (Blake, 1964). Along the contact and in blocks caught in the intrusion, hornfelsed shale consists of quartz-diopside-plagioclase-sphene ± grossularite garnet, and the limestone skarn is calcite-diopside-forsterite (Blake, 1964). Tungsten skarns along the southern edge of the intrusion and the Top pit (see below) are calcite-garnet-epidote-sphene (Hitchborn et al., 1996; this study).

Quartz-feldspar porphyry, mafic and lamprophyre dikes and sills cut the Bald Mountain pluton, its metamorphic

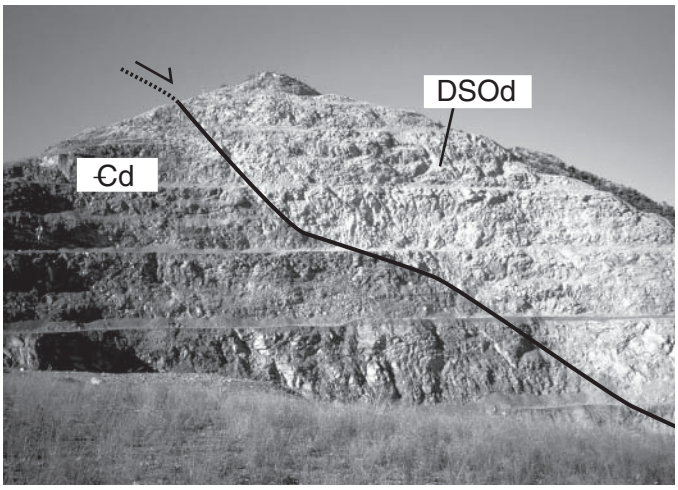

FIG. 6. The Ruby fault exposed in the Rat pit (outlined in Fig. 4). DOSd = Devonian to Silurian dolomite, undivided; Cd = Cambrian Dunderberg Formation. Benches are 40 ft.

aureole, and the surrounding rocks (Blake, 1964). Along the Bida trend, dikes and sills cut Cambrian to Mississippian rock. Lamprophyre inclusions in the pluton and inclusions of the pluton in the lamprophyre suggest that lamprophyre intrusions preceded, accompanied, and followed pluton emplacement (Blake, 1964; Hitchborn et al., 1996). Mortensen et al. (2000) sampled a variety of dikes and sills in the Bald Mountain area, and U-Pb analyses of zircons show that they were emplaced during a maximum period of about 9 m.y., between 159 to 150 Ma (see ages in Mortensen et al., 2000) and perhaps a much shorter period. Nutt et al. (2000) used immobile element plots of altered dikes and pluton from Bald Mountain to show that all the sampled intrusions are geochemically distinct from Tertiary rhyolite along Mooney Basin, consistent with a Jurassic intrusive event.

A 3- to 8-m-thick aplite sill that crops out only on the west side of Big Bald Mountain, at or near the contact between the Middle Cambrian Geddes Formation and the Secret Canyon Shale and in the 3 pit, yielded a ^{207}Pb-^{206}Pb date on zircon of 185.9 ± 3.8 Ma (Mortensen et al., 2000). The apparent age and immobile element ratios of this intrusion are distinct from those of other intrusions in the Bald Mountain area (Nutt et al., 2000).

Whole-rock Al, Ti, and Cr data suggest significant compositional variability among the pluton and dikes in the Bald Mountain area (Nutt et al., 2000), but immobile element ratios suggest that they are comagmatic. Chromium contents of the Bald Mountain intrusive rocks are highly variable (~1,500 ppm in an ultramafic dike in the 3 pit, 250 ppm in lamprophyre dikes at LJ Ridge, and 10 ppm in the Bald Mountain pluton). Despite the variation in Cr contents, the other immobile elements (Zr, Al, Ti, and P) retain fairly constant interelement ratios, which suggest that all these rocks are related.

Outcrops of the Bald Mountain pluton are characterized by coarse-grained phenocrysts of pink potassium feldspar, white plagioclase, rounded quartz eyes, and minor hornblende in a matrix of fine-grained quartz and biotite (Fig. 7A). It is classified as an I-type granite. Potassium feldspar and quartz phenocrysts are ragged and resorbed in places. Samples that

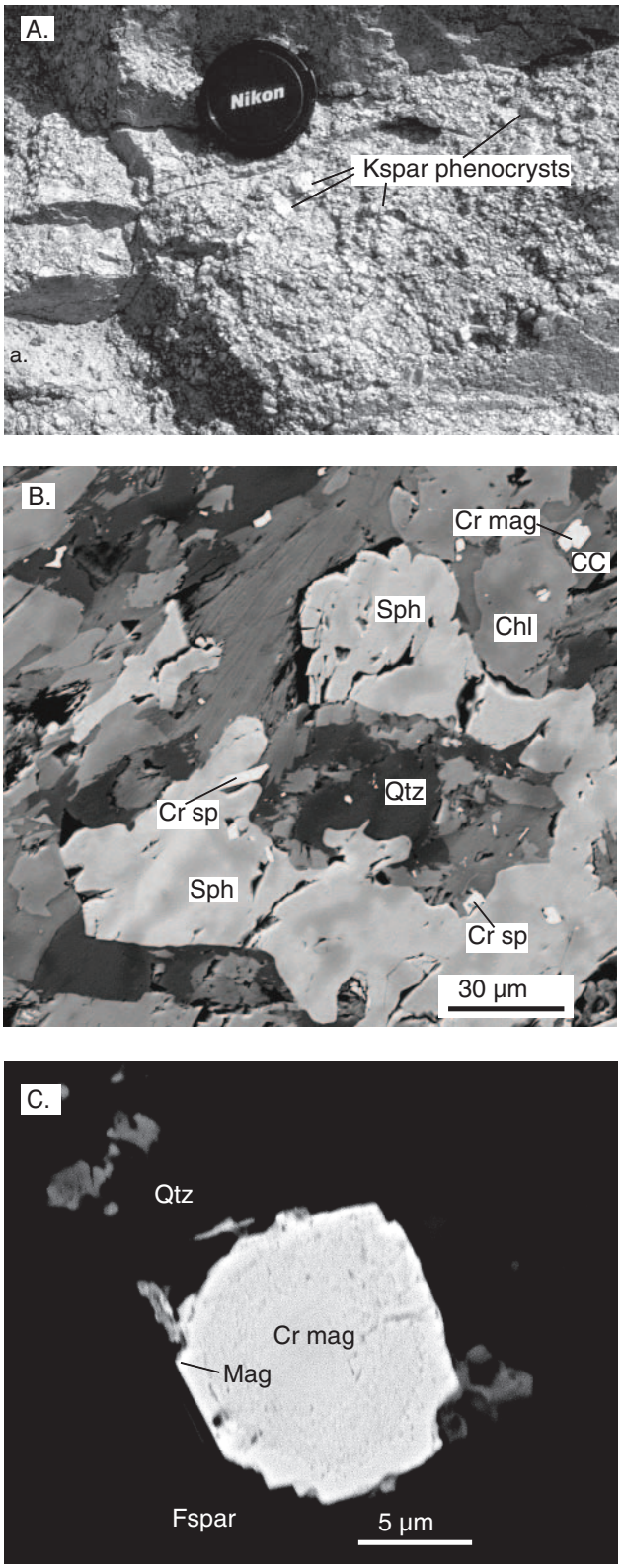

FIG. 7. Photomicrographs showing features of the Bald Mountain pluton. A. Bald Mountain intrusive rock with centimeter-size potassium feldspar phenocrysts. B. Scanning electron microscope (SEM) backscatter image of Cr spinel in quartz monzonite. C. SEM backscatter image of magnetite rims on Cr magnetite in lamprophyre. Bio = biotite, Cc = calcite. Chl = chlorite, Cr mag = Cr-magnetite, Cr sp = Cr-spinel, Fspar = feldspar, Qtz = quartz, Sph = sphene.

appear unaltered contain minor secondary chlorite ± epidote after biotite and hornblende, sericite ± clays after feldspars, and minor secondary dolomite, calcite, clay, barite, and titanium oxide. Accessory minerals include allanite, thorite, titanite, apatite, zircon, rutile, monazite, pyrite, and Fe-Ti oxides. Allanite and titanite are euhedral to subhedral in a fine-grained quartz matrix, apatite occurs as euhedral, rounded, and acicular grains, and monazite and thorite are small and identified only by scanning electron microscopy (SEM). Clots of secondary Ti oxide are abundant and commonly surround titanite. The lack of Fe oxide minerals is striking; the rocks contain <1 vol percent ilmenite and magnetite is only rarely present.

Euhedral to anhedral grains of ilmenite replace biotite and are present as inclusions in potassium feldspar phenocrysts and as isolated grains. In places, ilmenite contains rutile lamellae. The ilmenite is consistently Mn rich (4.5–7 wt % MnO by semiquantative energy dispersive, SED-EDS analyses). Mn enrichment in ilmenite occurs during late-stage differentiation and in more evolved rocks (Frost and Lindsley, 1991; Feenstra and Peters, 1996). Ilmenite is commonly mantled by titanite, which is thought to form during cooling of the rock (Ague and Brimhall, 1988a, b). The presence of ilmenite and scarcity of magnetite suggest that the intrusion solidified at least partly under reducing conditions; titanite formed during late cooling and oxidization.

Magnetite, though scarce, occurs in a variety of forms. It may be euhedral to subhedral and is enclosed in potassium feldspar and quartz phenocrysts. It rarely includes subsolidus oxidative solution lamellae of ilmenite. Its presence in phenocrysts indicates early crystallization. Most magnetite in the intrusion is nearly stoichiometric Fe_3O_4 with little to nil substitution by other siderophile elements, on the basis of SEM-EDS analyses. One sample of quartz monzonite contains Cr-rich magnetite and Cr spinel (Fig. 7B) as well as Fe-rich magnetite. The lamprophyre dike contains titanomagnetite and Cr magnetite surrounded by an Fe-rich rim (Fig. 7C).

The paragenesis of the accessory and oxide mineralogy suggests that conditions under which the magma solidified changed from oxidizing to reducing. The characteristics of the Bald Mountain pluton contrast with most paramagnetic intrusions, which are peraluminous and have low contents of Mn in ilmenite, white potassium feldspar, and no primary titanite (Clark, 1999). The apparent change in magma oxidation state may result from country rock assimilation. Ague and Brimhall (1988a, b) determined that in the western Sierra Nevada and Peninsular Ranges, California, reduced I-type intrusions that intruded graphitic pelites were reduced because of assimilation of pelitic material. We suggest that the reduced character of the Bald Mountain intrusive complex similarly resulted from assimilation of surrounding Cambrian carbonaceous sedimentary rocks. In addition, the presence of Cr spinel and Cr-rich rims on magnetite in a pluton with abundant primary allanite and thorite and the rimming of Cr magnetite by magnetite in lamprophyre suggest local magma mixing or assimilation involving the quartz monzonite and more mafic igneous rocks exposed in the area. An initial $^{87}Sr/^{86}Sr$ value of 0.7104 (Wooden et al., 1999) for the Bald Mountain pluton is elevated but is within the range for Jurassic plutons for the eastern Great Basin (Wright and Wooden, 1991). This value suggests significant crustal interaction and/or a source different from that of most Jurassic plutons in the eastern Great Basin.

Lead isotope data (Fig. 8) show that the Bald Mountain pluton is isotopically similar to other Jurassic plutons (Wright and Wooden, 1991) but is distinctly different from Cretaceous plutons derived from crustal melts. Values for $^{206}Pb/^{204}Pb$ and $^{208}Pb/^{204}Pb$ fall within a narrow range (Tosdal et al., 2000) that includes the Carlin trend and indicates a source region including continental crust, subcontinental mantle, and mantle-derived mafic components. Wright and Wooden (1991) interpret Sr, Nd, and Pb isotope data from plutons in northern Nevada to indicate that Jurassic magma is dominated by a subcontinental lithospheric mantle component that includes only a limited crustal component. King et al. (2004) used oxygen isotope values of zircon from plutons to suggest that the crustal component is greater in intrusions of the eastern Great Basin which is underlain by continental crust. This interpretation is supported by high oxygen isotope values (11.7–12.0‰) of quartz phenocrysts from a Bald Mountain porphyry dike (see below). Vikre (2000) also proposed extensive crustal contamination to explain the presence of sedimentary-derived S and Pb in Jurassic plutons in the eastern Great Basin. Sulfur isotope data for ore minerals show values similar to that of pyrite in the Cambrian Secret Canyon Shale (see below for detail) and suggest that the Bald

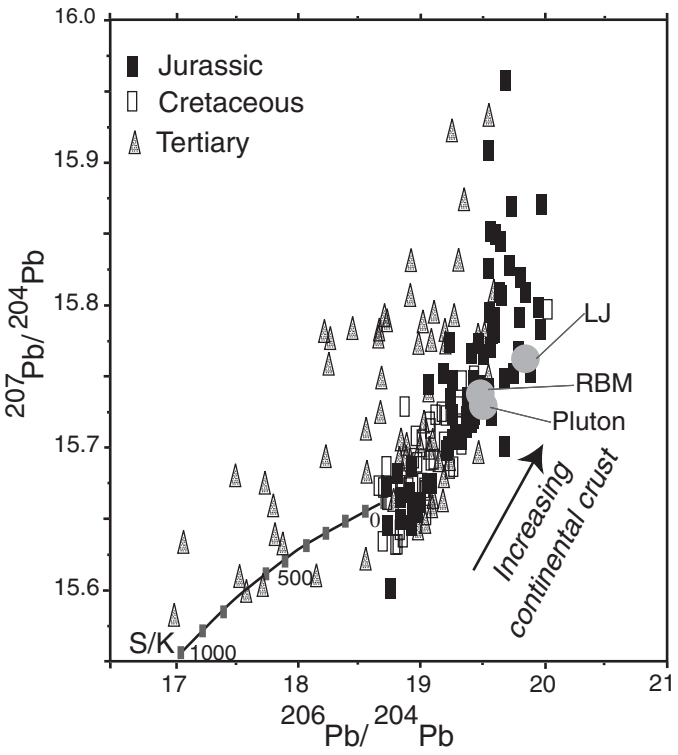

FIG. 8. Lead isotope compositions of potassium-feldspar phenocryst in the Bald Mountain pluton relative to Jurassic, Cretaceous, and Tertiary igneous rocks in Great Basin. Lead isotope compositions of stage 1 pyrite from the shallow RBM deposit and stibnite from the peripheral LJ Ridge deposit are similar to that of potassium feldspar, suggesting that Pb in the ore deposits is derived primarily from Jurassic igneous rock. Constructed from data in Nutt et al. (2000) and Tosdal et al. (2000).

Mountain pluton assimilated sulfur from Cambrian and Neoproterozoic sedimentary rocks and cycled sulfur into magmatic hydrothermal fluids.

Regional Geologic Setting in the Jurassic

During the Jurassic, what is now northeast Nevada was in a continental back-arc setting well east of the main magmatic arc and subduction zone to the west. Ward (1995) emphasized that subduction under western North America during the Mesozoic was cyclic and accompanied by compressional, extensional, and transpression and/or transextensional deformation. In the northeastern Great Basin, the Late Jurassic was a period of easterly directed compressive deformation (Thorman et al., 1991; Miller and Hoisch, 1995). Widespread magmatism between 165 and 150 Ma (Elison, 1995; Miller and Hoisch, 1995) resulted in emplacement of numerous plutons.

Jurassic-Triassic sedimentary rock, which probably overlay the Bald Mountain area at the time of pluton intrusion, is preserved in a syncline at Curie, Nevada (Fig. 1A). There, nonmarine strata, interpreted as a thin section of Upper Triassic Chinle Formation and Lower Jurassic Aztec Sandstone, overlie the marine Triassic Thaynes Formation. To the east, in Utah, these units accumulated in great thickness. Late Jurassic volcanic rocks similar to those in the Pinon Range may have overlain these Mesozoic rocks. In contrast, to the west (Yerington district and Humboldt complex), the Triassic-Jurassic rocks in the area of the more oxidized and sodic-altered Jurassic hydrothermal systems were deposited in a marine evaporite basin, which is interpreted to have been the source of basinal brines that were incorporated in hydrothermal fluids (Dilles et al., 2000).

Jurassic reconstruction

A Jurassic reconstruction of the Bald Mountain area is based on the estimated thickness of Paleozoic, Triassic, and Lower Jurassic rocks, the interpreted tectonic setting, an estimation of structural thickening, and conodont color alteration indices (CAI). Hornblende geobarometry was attempted, but the data are ambiguous. The depth due to stratigraphic burial is considered to be a maximum because of the possibility of Jurassic or older structural thinning or erosion prior to emplacement of the pluton. Sedimentary rocks exposed in the Bald Mountain area include the upper part of the Cambrian Eldorado Limestone through Mississippian Diamond Peak Formation (Fig. 5). Pennsylvanian to Mississippian Ely Limestone is exposed in the Alligator Ridge area and has a thickness estimated by Rigby (1960) of about 0.4 km. The thickness the Permian Rib Hill-Arcturus Limestone (1.4 km) is estimated from the Maverick Springs Range as reported in Hose and Blake (1976); the thickness of the Park City Group (0.4 km) is from Hose and Blake (1976) and Zamudio and Atkinson (1995), and the thickness of the Upper Triassic and Lower Jurassic units (0.2 km) is from Johnson et al. (1993) and Lucas and Goodspeed (1993).

Stratigraphic reconstruction suggests that as much as 6.7 km of Cambrian through Jurassic strata initially overlay the Bald Mountain intrusion, which corresponds to a lithostatic pressure of about 1.8 kbars (assuming 3.74 km/kbar for carbonate-rich crust, ±0.5 kbar or 1.9 km, as used by Miller and Hoisch, 1995). This pressure is consistent with the fact that the Lower Cambrian Secret Canyon Shale, which is the oldest clastic formation exposed, shows only incipient phyllite formation (Bucher and Frey, 1994, p. 193). The depth of intrusion emplacement at the Top deposit was a maximum of 5.5 km (stratigraphic thickness to the base of the Pogonip Group), which corresponds to a lithostatic pressure of 1.5 kbars. Assuming a geothermal gradient of 25°C/km, the maximum depths of 6.7 and 5.5 km correspond to temperatures of about 170° to 140°C.

Conodont color alteration indices (CAI) of rocks outside the thermal aureole are consistent with the inferred 25°C/km geothermal gradient (A. Harris, U.S. Geological Survey, pers. commun., 2001). A CAI of 1.5 for the Joana Limestone gives a burial depth of about 3 km and a temperature of <90°C, compared to a maximum of 3.4 km as indicated from stratigraphic thickness and a corresponding temperature of 85°C. This difference may be due to Jurassic or older low-angle faults that attenuate the section, episodes of erosion, or the uncertainty in the CAI.

The Jurassic tectonic setting at Bald Mountain is interpreted as being dominated by opening of the northwest Bida trend crustal structure during Mesozoic easterly directed compression. As described earlier, the en echelon pattern of faults, the localization of the intrusion within the trend, and the magnetotelluric (MT) evidence for a deep crustal structure suggest that it was probably a strike-slip fault with magma ascending along a pull apart. Miller and Hoisch (1995) suggested a similar setting for other Jurassic intrusions, many of which are aligned along northwest trends.

Bald Mountain Deposits

Mineral paragenesis and alteration studies of the Bald Mountain district are hampered by deep and pervasive weathering and oxidation of ore. Primary relationships are obscured in most places by supergene argillic alteration. Thus, descriptions that follow rely on our observations from isolated occurrences of unoxidized or partially oxidized material and previous observations reported in Blake (1964), Hitchborn et al. (1996), and Nutt et al. (2000). All Au production from the district is from oxide ores. Most refractory sulfide material is uneconomic due to its depth and the high costs of mineral processing and environmental controls. Figure 9 shows main features of the west side of the mining district.

The Bald Mountain hydrothermal system is exposed at two levels: in Cambrian-Ordovician rocks and Mississippian rocks (Fig. 10A). Most deposits are exposed at the deep level and fit into a concentric mineral and geochemical zonation pattern around the Bald Mountain pluton (Nutt et al., 2000, fig. 8). Mineralization at the shallow level is restricted to a single deposit (RBM), which we propose was dropped down from above the Top deposit by the Ruby fault. RBM is within and adjacent to a fine-grained quartz-feldspar-biotite porphyry intrusion inferred to be an apophysis of the Bald Mountain intrusive complex. Alteration and mineralization in deposits at the deep and shallow levels of exposure are described below (Table 2). Trace element compositions of ore minerals determined by electron microprobe and laser ablation-ICP-MS also are described. This is followed by a synopsis of fluid inclusion petrography and isotopic information on the deposits.

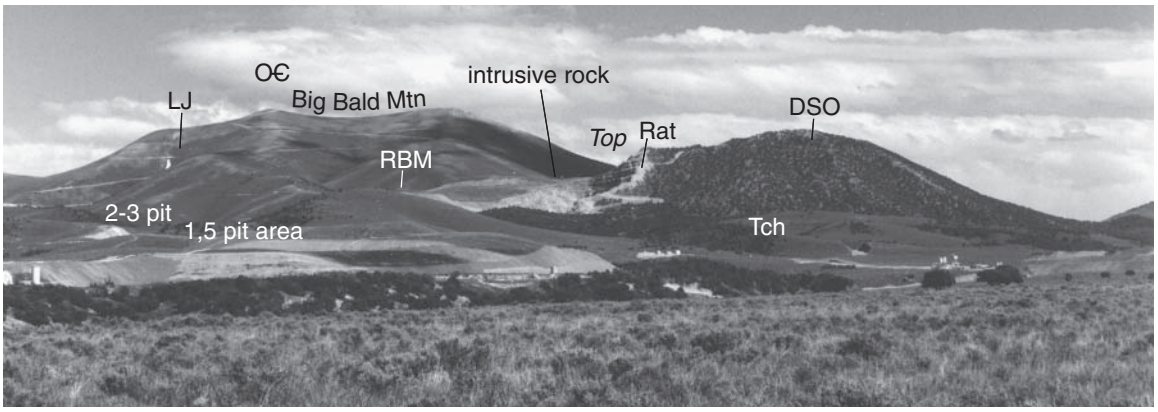

FIG. 9. Photograph of the west side of the Bald Mountain mining district, looking east. Tch = Tertiary chaotic unit of blocks of Ordovician through Eocene-Oligocene rocks overlain by debris flows, on the downthrown side of the Ruby fault, and making up low hills. The RBM pit is within the chaotic zone in a block of Mississippian rock. DSO = Devonian, Silurian = Ordovician dolomite, undifferentiated. O€ = Ordovician-Cambrian rocks that underlie Big Bald Mountain. LJ = site of LJ Ridge pit. The Top deposit is not shown on the photograph but is located, just out of sight, in the saddle area behind the Rat deposit; 1-5 and 3 pits are in Cambrian rocks.

Central deep levels of exposure

Cambrian to Ordovician sedimentary rocks and Jurassic intrusive rock are exposed in the deepest ore zones. This part of the system, mined for Au, includes Cu and W skarn and Cu and molybdenite veins, but the concentrations of Cu, W, and Mo are low compared to porphyry Cu-Au deposits. The central deposit, Top, is within the contact metamorphic aureole of the pluton, whereas the other deposits are outside the metamorphic albite-epidote hornfels facies aureole in which original bedding is generally well preserved (Blake, 1964).

In the central part of the system, at the largest deposit to date (Top), ore is hosted in Jurassic intrusive rock, skarn (diopside-garnet), hornfels, and marble of the Pogonip Group and Windfall Formation (see Hitchborn et al., 1996, for cross section of the Top deposit). Alteration is intense in the pit, but the Pogonip Group sandy limestone can be identified (Nutt and Hart, 2004) because it is decalcified and occurs as sand in the pit. The underlying Bullwacker Member of the Windfall Formation has karst breccia that hosts mineralization. Ore minerals occur in veins and disseminations in altered rocks. Alteration minerals include sericite and, by far the most common, supergene kaolinite (discussed below). Silicification is rare and mostly in hornfels and skarn. Where not obscured by kaolinite alteration, the Jurassic intrusion contains sparse, 0.5- to 2-mm quartz-molybdenite veinlets with potassic alteration envelopes. The pluton also is cut by wider (1–2 decimeter) northeast- and northwest-striking milky quartz veins and veinlets with phyllic alteration envelopes containing pyrite, chalcopyrite, silver sulfosalts, stibnite, and native Au. Milky quartz veins with low sulfide contents transect the contact metamorphic aureole and several extend outward into sedimentary rocks. Some of these quartz veins contained enough Au (0.919 oz/t) and Ag that they were exploited by miners in the early 1900s. Hornfels and marble are cut by north-striking, almost completely oxidized, millimeter- to centimeter-wide, chalcopyrite (±bornite) veins. Early miners reported high Cu (4 wt %) and Au (0.5 oz/t) in these veins, and Cu, Bi, Au, and Ag abundances show strong positive correlations

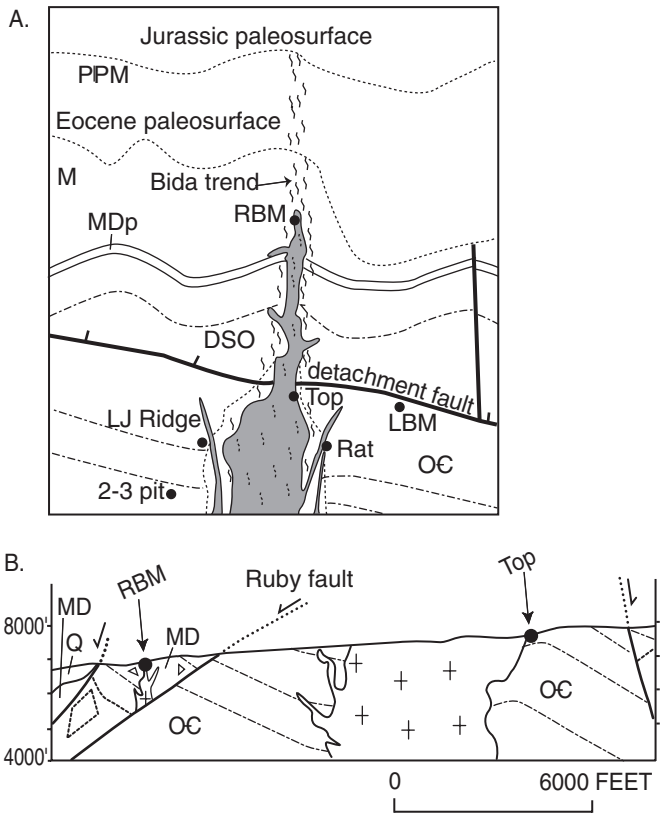

FIG. 10. A. Jurassic-age schematic model of the deposits in the Bald Mountain district. The Jurassic intrusion was emplaced along a crustal structure shown by wavy lines. RBM is in the upper part of the intrusion. Alteration or epithermal deposits in Jurassic rock have since been eroded. The diagram shows as much as 6.7 km of strata to the Jurassic surface. B. Schematic cross section between the Top and RBM deposits, showing that the block of Mississippian rocks which host RBM was dropped down from above the Top deposit. The cross section is east-west, looking north, from near the RBM deposit to the Top deposit marked in the geologic map (Fig. 4).

TABLE 2. Ore and Alteration Minerals of Bald Mountain and Jasperoid Discussed in the Text

Top deposit	Associated ore minerals	Alteration
Diagenetic, preore		Barite
Early ore	Arsenopyrite, pyrite, chalcopyrite, galena, sphalerite	Sericite, minor silicification
Main ore	Brassy pyrite, arsenopyrite, chalcopyrite, native Au, Ag sulfosalts, molybdenite, stibnite, Bi minerals, W minerals (skarn)	Sericite, dolomite, milky quartz veins, decalcification
Postore	Coarse-grained zoned pyrite	
Supergene		1A-kaolinite
Rat deposit		
Preore, not related to mineralization		Concordant silicification at the Hamburg/ Dunderberg contact
Main ore	Au-bearing jasperoid along dike edge, pyrite, arsenopyrite, sphalerite, galena, tetrahedrite, stibnite	Sericite, discordant silicification, milky quartz veins, calcite
Supergene		1A-kaolinite
LJ deposit		
Preore, not related to mineralization		Concordant silicification at the Hamburg/ Dunderberg contact
Main ore	Au-bearing jasperoid along dike dege, pyrite, arsenopyrite, sphalerite, galena, tetrahedrite, stibnite	Sericite, discordant silicification, drusy quartz, calcite
Supergene		1A-kaolinite
RBM deposit		
Early ore	Pyrite, chalcopyrite	Milky quartz vein, sericite envelopes
Main ore	Native Au, pyrite, sphalerite, molybdenite, chalcopyrite, Bi sulfide minerals, tetrahedrite, arsenopyrite, galena, and trace amounts of pyrrhotite, bornite, and stannite	Sercite and dickite, decalcification, minor silicification, milky quartz veins
Postore	Botryoidal and dendritic, very fine grained pyrite, and, to a lesser amount, marcasite	
Supergene	±pyrite or marcasite below the oxidation front	1A-kaolinite
Jasperoid, along main haul road to Top and in Bourne Canyon at the southern end of the district		
Postore		Discordant silicification along the Ruby fault

(Hitchborn et al., 1996). Garnet-diopside skarn at Top, as well as on the western edge of the pluton at the Zed skarn, was mined for W and contain scheelite, molybdenite, chalcopyrite, pyrrhotite, sphalerite, and minor ilmenite and sphene, as well as traces of cassiterite. In the extensions of the Top deposit (Mahoney and Sage Flat; Fig. 2), stockwork and disseminated Au ores contain less Cu and are variably enriched in Mo, Sn, Bi, Te, Pb, Zn, Ag, As, Sb, Hg, and Tl (Table 1). In these pits, the pluton exhibits an early stage of sericitic alteration followed by a later stage of minor illite-smectite and smectite, and supergene argillic alteration characterized by 1A kaolinite.

Hydrothermal magnetite and anhydrite, which are common in many porphyry copper and skarn deposits, have not been reported in the Bald Mountain area (Table 3). Although barite is present in silicified hornfels on the north side of Top, its textures and sulfur isotope composition indicate a diagenetic origin (discussed below). Fluorite, which is common in some W skarn and porphyry Mo systems, has not been reported in the Bald Mountain area. The absence of these minerals indicates that the ore fluids were reduced and lacked significant sulfate or fluorine. The presence of pyrite and dolomite in phyllically altered parts of the pluton are evidence that the ore fluids contained H_2S and CO_2.

A small pocket of unoxidized mineralized rock was exposed by mining of the Top deposit. Although this material is not ore grade, the samples provide an indication of mineralogy. They consist of quartz-sericite–altered intrusive rock with disseminated pyrite, arsenopyrite, and minor amounts of galena, sphalerite, and chalcopyrite. Some of this rock contains abundant disseminated pyrite. Sericite is the most abundant alteration silicate, but fine-grained 1A kaolinite also is present in the matrix. Sericite from one of these samples yielded an $^{40}Ar/^{39}Ar$ age of 157.1 ± 0.9 (A. Iriondo, U.S. Geological

TABLE 3. Some Characteristics of Bald Mountain and Porphyry-Related deposits

Bald Mountain	Porphyry-related Au [1]
Rare magnetite except in lamprophyre dikes	Hydrothermal magnetite
Au-Bi association	Cu-Au association
W skarn	Cu-Au skarns
Cu historically mined from veins	Open-pit mining for Cu
Sulfide poor, low fs_2	Sulfide rich
No anhydrite	Anhydrite
δS^{34} of metals and pluton >15 (sulfur derived from sedimentary rocks)	δS^{34} about 0 (sulfur derived from magmatic source)
No fluorite	Fluorite

[1] Porphyry-related Au from Sillitoe (1997) and Babcock et al. (1995)

Survey, writ. commun., 2003) that is similar to the best zircon U-Pb ages for the pluton (159.0 ± 0.5 Ma) and quartz-feldspar porphyry dikes (159.0 ± 0.7 Ma; 158.9 ± 0.7 Ma; Mortensen et al., 2000). The $^{40}Ar/^{39}Ar$ age also indicates that the hydrothermal system was shallow enough to cool through the blocking temperature for sericite of ≤350°C (McDougall and Harrison, 1988; L.W. Snee, U.S. Geological Survey, pers. commun., 2006) soon after pluton emplacement.

Arsenopyrite and pyrite are the most abundant sulfide minerals in the unoxidized sample from the Top deposit, and the assumption is made that they were abundant in the orebody prior to supergene oxidation. Arsenopyrite is euhedral and coarse- to fine-grained (Fig. 11A); the fine-grained arsenopyrite mainly occurs in aggregates. Two generations of pyrite were identified. The early generation, contemporaneous with arsenopyrite, is subhedral and medium- grained, whereas the later generation is finely zoned, fine- to medium-grained and commonly occurs in coarse aggregates (Fig. 11B). Marcasite is associated with late pyrite. Sericite inclusions indicate that the sericite predates the later generation of pyrite. Gold was detected in both the arsenopyrite and early pyrite by LA-ICP-MS. Early-stage, coarse- and fine-grained euhedral arsenopyrite grains contain as much as 38 ppm Au. Early subhedral pyrite contains as much as 25 ppm Au. Late pyrite has distinctive chemistry (Fig. 12). It is the only Fe sulfide mineral analyzed that contains Tl (to 1,000 ppm) and Hg (to a few hundred ppm). Gold generally is absent. The most consistent elemental correlation in this pyrite is As, Sb, Tl, and Hg, which suggests either that the late pyrite was deposited during the waning period of Jurassic mineralization or, more likely, during a subsequent period of hydrothermal activity.

Drilling in the vicinity of the Sage Flat area, just south of the Top deposit and covered by alluvium, encountered a variety of ore minerals, including a number of Bi minerals (Placer Dome, unpub. mineralogy data., 2003) such as native Bi, bismuthinite (Bi_2S_3) and tellurobismuthinite, as well as Bi oxide,

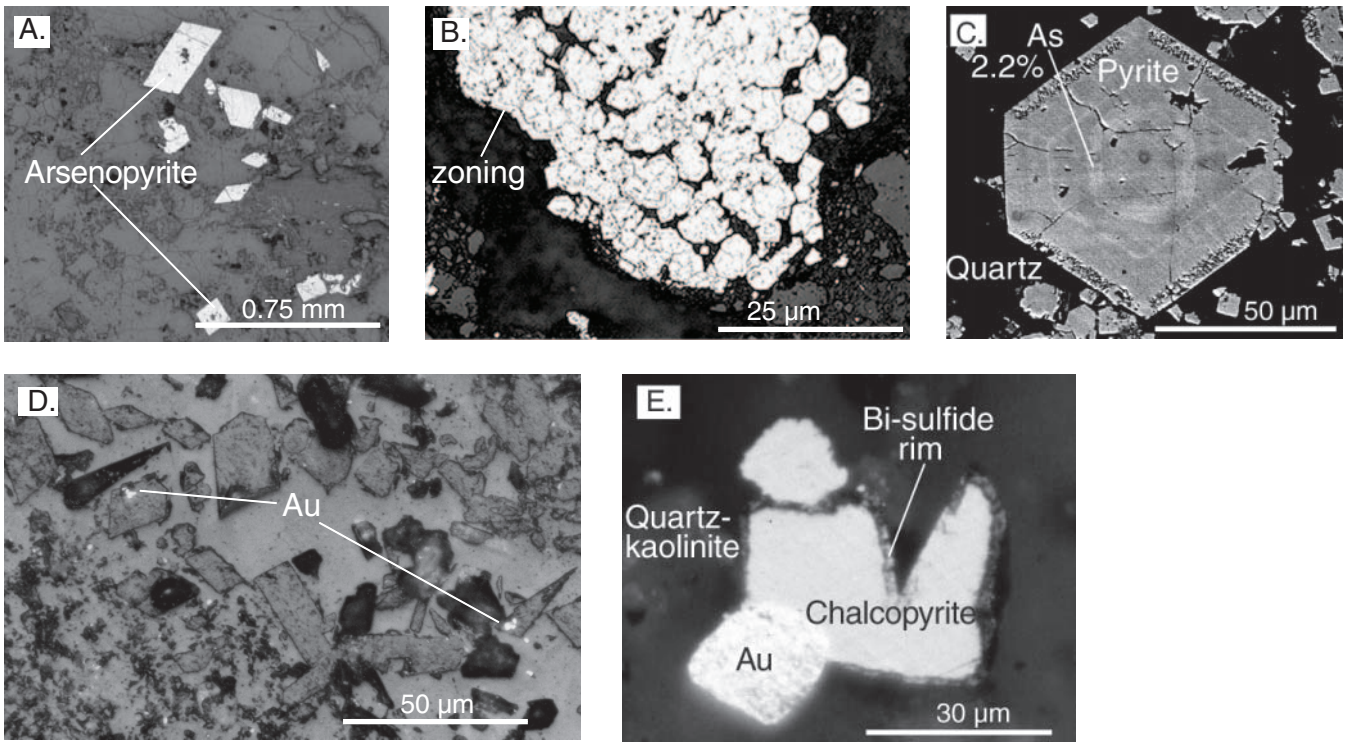

FIG. 11. Petrographic and SEM backscattered electron images of samples from deposits. A. Euhedral arsenopyrite from the sulfide zone of the Top deposit. B. Photomicrograph, in reflected light, of an aggregate of late, euhedral zoned pyrite from the Top deposit. C. SEM backscattered electron image of zoned pyrite from the Rat deposit. The pyrite contains as much as 2.2 wt percent As. D. SEM backscattered electron image from the LJ Ridge deposit, showing native Au in oxidized euhedral arsenopyrite; unoxidized arsenopyrite contains up to 8,500 ppm Au (Fig. 12C). E. Reflected light photomicrograph of native Au and chalcopyrite rimmed by Bi sulfide minerals in argillic-altered host from the RBM deposit.

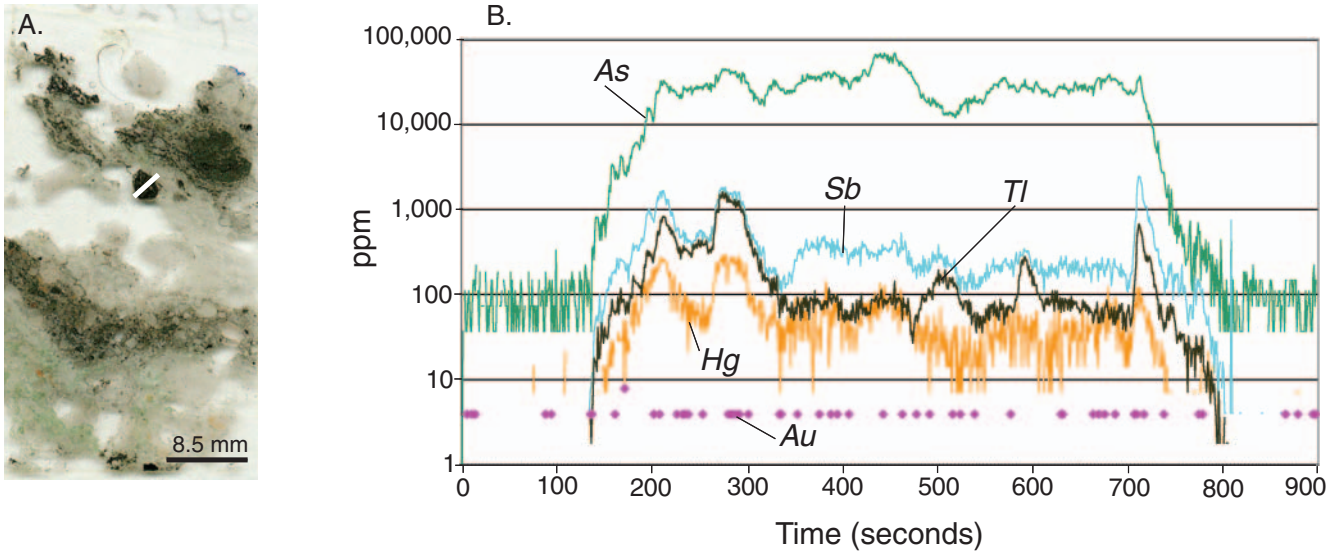

FIG. 12. LA-ICP-MS profile of an aggregate of pyrite in thin section. A. Thin section with an aggregate of late, zoned pyrite in a small sulfide zone at Top; part of the aggregate of pyrite is shown in Figure 11B. White line crossing aggregate of pyrite is the approximate scan line profile shown in (B). B. LA-ICP-MS scan across aggregate of pyrite. On this and following profiles, Y axis is abundance in ppm; X axis is time as laser crosses mineral and therefore shows changes in composition across the grain. The LA-ICP-MS technique used here is described by (Ridley, 2000).

sulfate, and carbonate minerals that presumably formed by supergene processes. Other minerals include native Au, petzite ($AuAg_3Te_2$), electrum, native Ag, galena, arsenopyrite, chalcopyrite, and sphalerite.

Peripheral deep deposits

The peripheral deep deposits, which include LJ Ridge, Rat, 1, 2-3, 5, and LBM (Fig. 2), share some features with polymetallic vein deposits (Cox, 1986), although the sulfides are associated with silicified carbonate rock rather than quartz veining. These deposits are outside the contact metamorphic aureole that surrounds the Bald Mountain intrusion and are hosted in Cambrian formations over a vertical stratigraphic interval of 1,250 m (Fig. 5). Ore is in jasperoid and, to a lesser amount, in quartz veins and veinlets in sericite and argillically altered rocks. In shales, ore is mostly restricted to narrow (1–5 m) silicified alteration zones along nearly vertical structures that are sometimes occupied by dikes of quartz-feldspar porphyry, as at Rat (Fig. 13; cross section shown in Hitchborn et al., 1996), or lamprophyre, as at LJ Ridge.

Rat and LJ Ridge are similar: both are at and near the Hamburg-Dunderberg contact, and the best ore zone is along dikes that cut across bedding. At these two deposits, ore extends outward from the vertical structures for 10 to 100 m. Petrographic examination of samples from Rat and LJ Ridge show an early stage of sericite alteration (Table 2), with or without dolomite or calcite, and a later stage of argillic alteration, similar to that at Top, that is largely supergene in origin.

Most ore-related jasperoid in these two deposits is discordant to bedding. Gold-bearing jasperoid occurs mostly along the edges of veins, faults, and dikes but locally extends outward in either the ore beds or adjacent limestones. However, there also is widespread strata-bound jasperoid at the contact between the Hamburg-Dunderberg (Rat and LJ Ridge) and Eldorado-Geddes (1–3 pits). These jasperoids are, in a few places, cut by intrusive rock and milky quartz veinlets which, along with isotopic data (see below), indicate that they were produced by an event that preceded emplacement of Jurassic intrusions and related hydrothermal activity (Fig. 5).

In the peripheral deep deposits, milky quartz veins and veinlets in sericite and argillically altered rocks typically contain variable amounts of pyrite, arsenopyrite, sphalerite,

FIG. 13. Photograph, looking east, showing approximate outline of dike in the Rat deposit. Gold ore is concentrated along edges of the dike. Bedding of host lithology, shown at top of photograph, strikes about north and dips eastward at about 20°. Benches are 40 ft in height. Photograph from Stephen G. Peters, USGS.

galena, tetrahedrite, and stibnite. Chalcopyrite is minor or absent and scheelite, molybdenite, and Bi minerals are absent. Disseminated ores contain pyrite and arsenopyrite and minor to nil base metal sulfide minerals. Pyrite is typically euhedral, a few millimeters to microns in size, bright and brassy in reflected light, homogeneous, or complexly zoned (Fig. 11C), with some zones containing as much as 4 wt percent As, as determined by microprobe. Although Hitchborn et al. (1996) reported late quartz with disseminated marcasite and Au in these deposits, we did not identify these minerals. All the peripheral deep deposits have much lower concentrations of W, Sn, Mo, Bi, Te, and Cu than those in the central part of the system (Table 1). They also have variable Au/Ag ratios. In the 1 to 3 deposits, As and Sb concentrations are high, and As, Sb, Au, and Ag exhibit strong correlations (Hitchborn et al., 1996). Structural relationships suggest that the 1, 2, and 3 deposits were originally a single deposit that was dismembered by younger faults, and drilling has intercepted Ag-bearing Pb-Zn veins below them.

LJ Ridge: The LJ Ridge deposit, in which ore is strata bound near the contact separating Hamburg Limestone and Dunderberg Shale and discordant along dikes, is 500 m from the metamorphic aureole and has the lowest base metal concentrations and highest Au/Ag ratio of any deposit in the Bald Mountain district (Table 1). This deposit most resembles a Carlin-type deposit and is therefore described in greater detail. The Dunderberg Shale is altered and mineralized adjacent to faults, one of which is filled by a lamprophyre dike. The lamprophyre dike was an unfavorable host for Au and is not silicified. However, it is altered to sericite and calcite and contains disseminated pyrite and arsenopyrite that replace magnetite. The dike is also cut by thin (<2 mm) calcite veins containing pyrite, arsenopyrite, chalcopyrite, sphalerite, tetrahedrite, and galena. Petrographic observations and geochemical data indicate that hydrothermal fluids introduced K to form sericite, CO_2 to form calcite, and H_2S to form sulfide minerals, but insignificant Fe was introduced (Nutt et al., 2000). The Dunderberg Shale at the deposit consists of calcite with variable amounts of sericite (2M1 mica), minor quartz, disseminated pyrite (dodecahedrons), and trace amounts of organic carbon. In mineralized samples, the calcite is variably recrystallized (with poikilitic textures), dissolved, or replaced by quartz. In some of the pervasively silicified samples sericite is coarser grained and is randomly oriented, suggesting recrystallization or neoformation. Such discordant jasperoid is commonly fractured or brecciated and cemented with drusy quartz.

All of the variably altered rocks contain disseminated euhedral brassy pyrite as well as arsenopyrite, which has an elongate habit and crystal aggregates that locally form radial sprays. The amount of disseminated pyrite and arsenopyrite ranges from <1 to as a much as 15 vol percent adjacent to veins. Altered rocks are cut by veins that contain drusy quartz (0.5–5 mm), arsenopyrite, pyrite (dodecahedrons), and stibnite, all of which are mantled by calcite.

Gold resides in arsenopyrite and pyrite, but not stibnite, regardless of whether these minerals are disseminated in altered rocks or present in veinlets (Fig. 14A). Electron microprobe analyses show that arsenopyrite contains as much as 0.57 wt percent Sb and 0.93 wt percent Au. Pyrite contains as much as 3.65 wt percent As, 0.31 wt percent Cu, 0.20 wt percent Sb, and 0.44 wt percent Au. LA-ICP-MS profiles of fine-grained arsenopyrite confirm the high Au contents (up to 0.43 wt %: Fig. 14B). Oxidized arsenopyrite (Fig. 11D) contains bright spots of native Au. Analyses of least oxidized pyrite show a correlation of Au (750 ppm) with S, Fe, As (to 1 wt %), Cu (to 500 ppm), Sb (to 3,000 ppm), Pb (to 100 ppm), Co (to 35 ppm), and Ag (to 30 ppm). Stibnite contains Sn (to 100 ppm) and Pb (to 2,000 ppm) but lacks Au. Whole-rock geochemical data indicate that both Fe and S were introduced to form the Au-bearing pyrite and arsenopyrite (Nutt et al, 2000).

Central shallow level of exposure

The RBM pit is in Jurassic intrusive rock and Mississippian sedimentary rocks and this deposit is interpreted as the upper part of the hydrothermal system that was faulted down after mineralization (Fig. 10B). The RBM deposit is localized by a fault that transects porphyry intrusive rock and Mississippian siltstone and shale. The intrusion in RBM was dated twice; a K-Ar age of 158.1 ± 5 Ma was obtained on biotite from a location about 900 m northeast of the RBM pit (Hitchborn et al., 1996) and an age of 169.4 ± 5 Ma was obtained on sericite from a late dike (Placer Dome, NA, unpub. data, 2003). The first date is considered the better of the two, but both indicate a Jurassic age.

The ore mineralogy and geochemical signature of the RBM deposit are similar to that of the Top deposit (Table 1), which suggests that it is a shallow expression of the same system. The deposit is at about the same stratigraphic level as the Eocene Carlin-type deposits in Mooney Basin and near Alligator Ridge, but its mineralogy and geochemical characteristics are distinct.

The sedimentary rocks are highly altered thin-bedded Chainman Shale. The contact between Chainman Shale and Diamond Peak Formation, marked by interbedded shale, sandstone, and conglomerate, is exposed at the top of the northeastern edge of the pit. Ore fills fractures and is disseminated in adjacent altered rocks. In the pit, rocks are pervasively oxidized and argillically altered (supergene), except for a small 3- to 5-m-wide area of sulfide-rich material in carbonaceous shale at the bottom of the pit. The deep part of the deposit is relatively unoxidized and drill core of mineralized porphyry, Chainman Shale, and an aphanitic dike (lamprophyre?) were available for study. Typical oxide ore at RBM has low Au/Ag ratios, variable Cu, Zn, and Pb contents, and high trace element concentrations (Table 1). Twenty-foot (6 m) blast holes locally encountered high-grade ores with as much as 5.5 oz/t (170 g/t) Au.

Alteration minerals (Table 2) include hydrothermal sericite, illite, and dickite, and supergene kaolinite. Unoxidized carbonaceous shale on the floor of the pit is pervasively sericite altered. We previously interpreted the kaolinite as hypogene (Nutt et al., 2000), but XRD studies show that the kaolinites analyzed are 1A type and unordered, and new δO and δH data (see below) indicate that it is supergene and overprinted an earlier alteration represented by sericite and dickite.

Three stages of alteration and mineralization were identified by petrographic and geochemical studies of unoxidized rocks. The first stage consists of milky quartz veins that

contain chalcopyrite and pyrite; relict sericite (2M1 mica) is present along vein margins. No native Au was detected in the veins that we sampled.

Most of the Au was introduced with a variety of base metal sulfide minerals during a second stage, associated with sericite and dickite alteration and silicification of sedimentary host rocks. The mineralization includes native Au with disseminated anhedral and cubic pyrite, sphalerite, molybdenite, chalcopyrite, Bi sulfide minerals, tetrahedrite, arsenopyrite, galena, and trace amounts of pyrrhotite, bornite, and stannite. Pyrite contents are variable and range from <1 to more than 50 vol percent. Other base metal sulfide minerals are usually present in amounts of <1 vol percent, with sphalerite being the most abundant. Grains of native Au (up to 1 mm) occur alone and intergrown with chalcopyrite (Fig. 11E), Bi-Cu (emplectite), and Bi-Pb-Cu (aikinite) sulfide minerals. Electron microprobe analyses show that native Au contains 2.71 to 3.18 wt percent Ag and 0.21 to 0.49 wt percent Cu. High concentrations of Au (4,400 ppm) are present in emplectite ($BiCuS_2$) along with 2.03 wt percent Zn, 1.79 wt percent Sb, and 0.70 wt percent As. In two small euhedral pyrite grains containing inclusions of galena and chalcopyrite, 780 and 1,020 ppm Au were detected. Both pyrite grains have low concentrations of As (2,000 and 300 ppm). The mineral assemblage at RBM is reminiscent of the strong geochemical correlation between Cu, Bi, Au, and Ag in the central deep Top deposit. As in the deep deposits, magnetite, anhydrite, and fluorite are absent.

Brassy pyrite was probably introduced early in the second stage. This pyrite is euhedral to subhedral and distinguished by its brassy color in hand specimen. No zoning is visible by microscopic examination, but zoning is apparent in the LA-ICP-MS profiles. Arsenic concentrations are about 1 wt percent, Pb is up to 5 wt percent, and Cu is up to 0.3 wt percent. Gold is distributed throughout the pyrite at concentrations as high as 90 ppm.

The third stage of mineralization and alteration consists of fine-grained, botryoidal or delicate dendritic pyrite (Fig. 15A, B), with lesser marcasite, which locally replaces early base metal sulfide minerals, especially chalcopyrite, in kaolinite-altered rock. The botryoidal pyrite and marcasite superficially resemble the sooty pyrite in Carlin-type deposits, but they are unlike the arsenian pyrite that rims earlier pyrite in typical Carlin-type deposits. Chalcopyrite, native Au, and Bi sulfide minerals are absent in samples that are pervasively overprinted by this pyrite and marcasite, except where they are preserved as inclusions.

The late-stage Fe sulfides formed either during collapse of the Jurassic hydrothermal system or during supergene alteration. Electron microprobe analyses show that late pyrite and marcasite generally contain more As, Sb, Pb, Cu, Ni, and Mn than earlier stages of pyrite. In places where chalcopyrite, Bi minerals, and galena are replaced by botryoidal Fe sulfides, Au correlates with elements such as Bi, Ag, Sb, Cu, Pb, and Sb. Gold concentrations also correlate with Sn (up to 250 ppm), Cs (up to 380) ±Mo, Cr, and Mn; these elements probably are absorbed or contained in minerals mixed with clay, phosphate and/or sulfate minerals. Unlike late pyrite at the Top deposit, Hg is absent, and Tl concentrations are low (Fig. 15C). Hitchborn et al. (1996) proposed that the late pyrite-marcasite stage introduced most Au, but we find little evidence to support that interpretation. Instead, our data suggest that the late pyrite formed by the destruction of early formed base metal sulfide minerals. Gold was locally remobilized but not introduced during this stage.

Fluid Inclusion Petrography

The types of fluid inclusions in quartz from the deep and shallow deposits are indicative of distinctly different environments (Hitchborn et al., 1996; Nutt et al., 2000; this study). In this study, representative samples containing quartz veins or quartz phenocrysts were collected from the RBM, LJ Ridge, Rat, and Top deposits for fluid inclusion petrography. Quartz phenocrysts from altered samples were studied because in other porphyry and epithermal systems they commonly contain secondary fluid inclusions that record the passage of hydrothermal fluids (e.g., Hedenquist et al., 1998). The petrographic studies consisted of documentation of fluid inclusion populations and their phase ratios (cf. Hedenquist et al., 1998; Lang et al., 2000) and crushing in oil to evaluate the presence or absence of high-pressure gas (cf. Roedder, 1984; Bodnar et al., 1985).

Fluid inclusions in milky quartz veins and quartz phenocrysts from the LJ Ridge, Rat, and Top deposits, which are from deep levels of the exposed igneous system, are similar: they lack daughter minerals and, based on the phases observed, are inferred to consist mainly of H_2O and CO_2. Three types of fluid inclusions were identified at room temperature: (1) three-phase aqueous liquid + CO_2 liquid + vapor inclusions, (2) two-phase aqueous liquid-rich inclusions, and (3) vapor-rich inclusions (Fig. 16A-C). The three types indicate that P-T conditions crossed a solvus in the CO_2-H_2O-NaCl system. The abundance of each type varies from the central to the peripheral parts of the system. All three fluid inclusion types are common in quartz phenocrysts from the Bald Mountain pluton and in milky quartz veins from proximal deposits. These fluid inclusions typically occur in secondary planes that contain only one inclusion type, but some planes contain liquid- and vapor-rich fluid inclusions. The planes with three-phase fluid inclusions have the most variable phase ratios, which suggest that these inclusions were necked following phase separation or heterogeneous trapping of immiscible fluids. As expected, upon crushing in oil, the quartz phenocrysts and milky quartz veins yield numerous large gas bubbles, which is clear evidence that the fluid inclusions contain significant amounts of gas (e.g., CO_2) at high internal pressure. After crushing, the gas bubbles formed in the oil remained constant in size, which indicates that the fluid inclusions lack appreciable oil-soluble CH_4. Hitchborn et al. (1996) found that milky quartz veins and quartz phenocrysts in dikes from the peripheral Rat and LJ Ridge Au deposits contain small equant to irregular secondary liquid-rich inclusions. At LJ Ridge, we observed both primary and secondary fluid inclusions in milky quartz veinlets that contain auriferous arsenopyrite and pyrite. Most of these fluid inclusions are liquid rich with vapor bubbles that occupy 10 to 20 vol percent of the inclusions. However, a few three-fluid phase inclusions containing liquid CO_2, and a few secondary planes of vapor-dominant inclusions were also observed. As for samples from the deep proximal part of the system, samples from LJ and Rat yielded large gas bubbles upon crushing in oil, which indicates the presence of large amounts of CO_2 at high internal pressure.

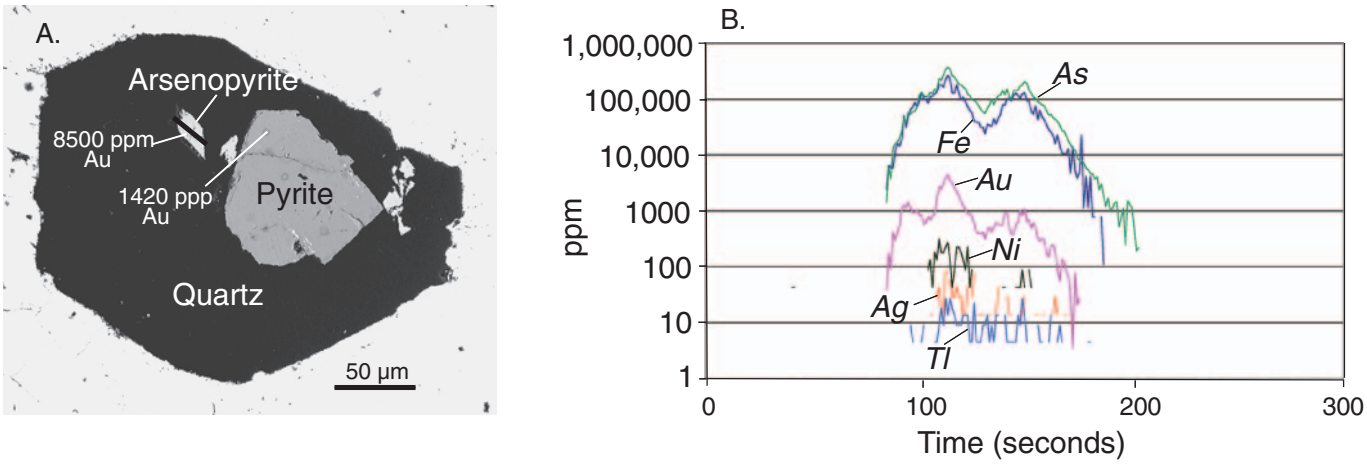

FIG. 14. LA-ICP-MS profile of Au-bearing arsenopyrite from the LJ Ridge deposit. A. SEM backscattered electron image of Au-bearing arsenopyrite with free Au and Au-bearing pyrite from LJ Ridge; later stibnite contains no Au. Black line crossing arsenopyrite shows location of the profile. B. LA-ICP-MS profile from arsenopyrite (A).

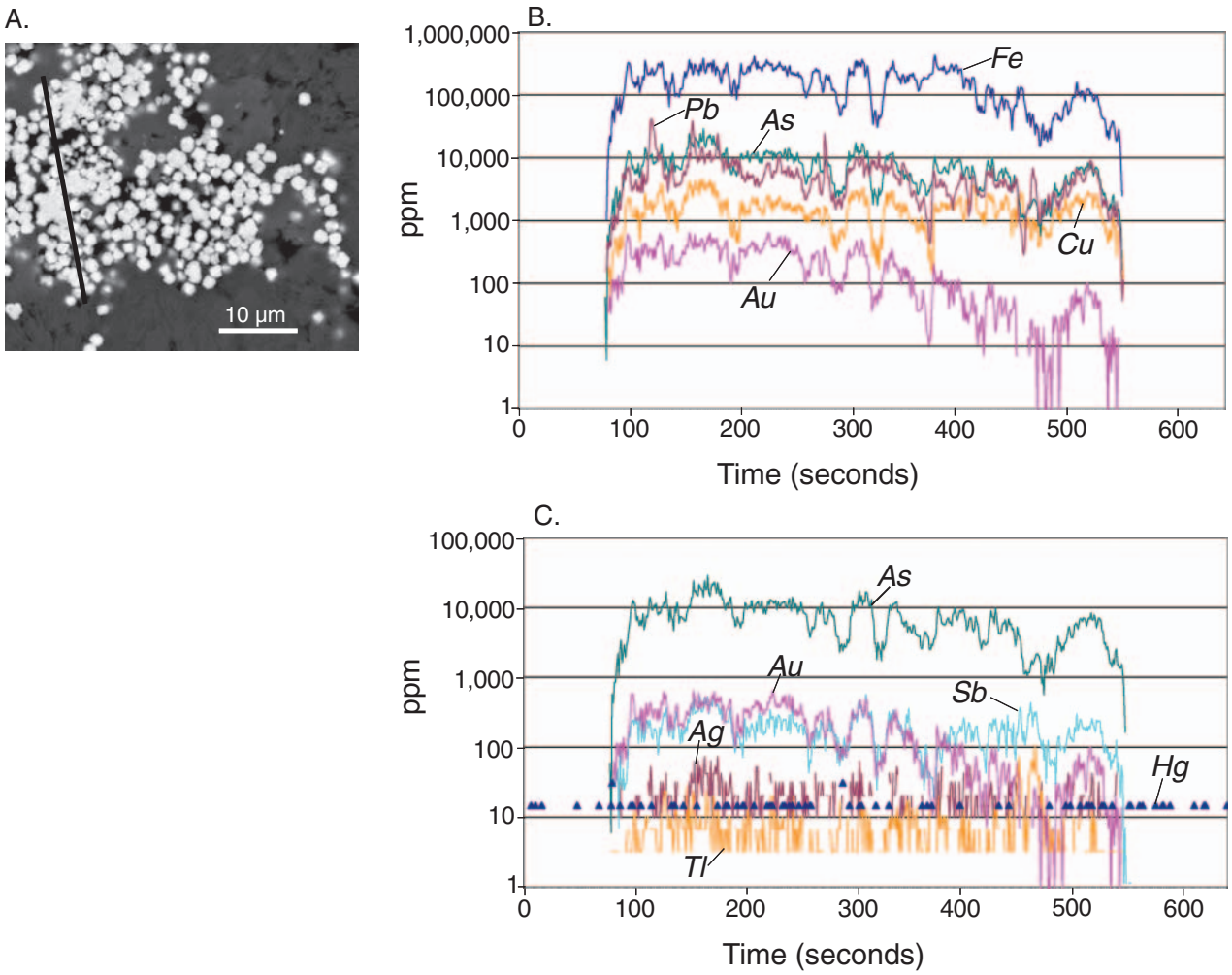

FIG. 15. LA-ICP-MS profile of late-stage botryoidal pyrite at RBM. A. Photomicrograph of late botryoidal pyrite with red line showing profile. B. Profile shows high Fe, Pb, Cu, As, and Au where pyrite replaces earlier base metal Au-bearing minerals. C. Profile shows low Tl and Hg; compare with late pyrite at Top (Fig 12).

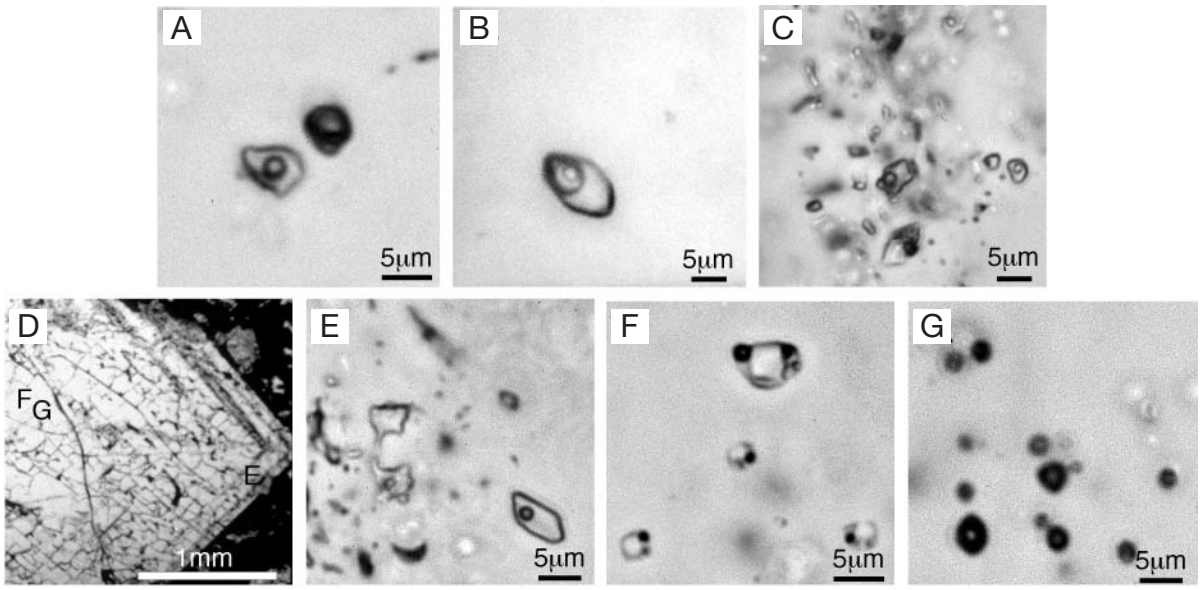

FIG. 16. Transmitted light photomicrographs of fluid inclusions. A. Secondary aqueous liquid-rich and carbonic vapor-rich fluid inclusions in quartz phenocryst from the Bald Mountain pluton. B. Secondary three-phase CO_2-H_2O inclusion in quartz phenocryst from the Bald Mountain pluton. C. Aqueous liquid-rich fluid inclusions in drusy quartz containing auriferous arsenopyrite and pyrite from the LJ Ridge deposit. D. Zoned quartz crystal from the RBM deposit spanning stages 1 and 2; locations of fluid inclusions shown in (E-G). E. Primary necked aqueous liquid-rich fluid inclusions in the rim of the zoned quartz crystal. F. Pseudosecondary hypersaline inclusions. G. Pseudosecondary vapor-rich fluid inclusions in the core of the zoned quartz crystal.

Fluid inclusions in milky quartz veins from RBM at shallow exposure levels are distinctly different (Fig. 16D-G). Quartz veins (with chalcopyrite and relict sericite) in argillically altered rocks contain abundant, small (<10μm), equant, secondary planes of hypersaline or vapor-rich fluid inclusions. The hypersaline inclusions contain vapor (10–15 vol %), halite (10–20 vol %), and commonly, one to three small unidentified daughter minerals. Hitchborn et al. (1996) noted similar fluid inclusions in quartz phenocrysts from a porphyritic dike at RBM, including some hypersaline inclusions with as many as 10 daughter minerals. We also studied milky quartz veins that contain planes of irregular vapor-rich fluid inclusions and planes of liquid + vapor inclusions with variable liquid to vapor ratios that appear to have resulted from necking down. One euhedral crystal of milky quartz exhibits pseudosecondary planes of hypersaline and vapor-rich fluid inclusions in the core and irregular liquid-rich inclusions along primary growth zones near the rim (Fig. 16D). These features are interpreted to indicate that, following an episode of boiling, either vapor condensate accumulated or meteoric water collapsed into the system. The former possibility is supported by the second stage of hypogene argillic alteration (dickite) with disseminated chalcopyrite and native Au, which likely formed where acid volatiles (e.g., HCl, H_2S, CO_2) condensed into local ground water. Upon crushing in oil, some of the quartz fragments from these veins yielded a few small gas bubbles, which suggests the presence of moderate amounts of CO_2 at moderate internal pressure.

The two-phase liquid-rich inclusions in the deep deposits appear similar to those in early deep quartz veins at Butte, Montana (with ~5 mol % CO_2 and 6 wt % NaCl), which formed at a pressure of about 2 kbars and a depth of 6 to 7 km (Bodnar, 1995; Rusk et al., 2004). In contrast, the paired hypersaline and vapor-rich inclusions observed at RBM are similar to those in much shallower porphyry systems such as Red Mountain, Colorado, which formed at pressures <1 kbar and depths of ~3 km (Bodnar, 1995). This depth is similar to the 2 to 3 km estimated by stratigraphic reconstruction for the RBM deposit. The crushing behavior of inclusions at RBM that suggested CO_2 in some of the inclusions at moderate internal pressure is normally not observed in epithermal vein deposits because of the low pressures and depths at which they form (Bodnar et al., 1985). Thus, RBM probably formed at a depth greater than those of most epithermal veins but at a much shallower depth than the deep deposits such as Top and Sage Flat. The moderate pressures and depths suggested here are consistent with the reconstructed 2- to 3-km depth of RBM below the Jurassic paleosurface but not with the shallow depths (<1 km) below the Eocene paleosurface (Fig. 10A).

The qualitative information and first-order interpretations presented here suggest that the deposits formed from magmatic fluids at two different pressures and depths, consistent with the 2.8-km stratigraphic separation between RBM and the deeper deposits and the Jurassic reconstructed paleodepths. The assortment of fluid inclusion types in the deep and shallow deposits at Bald Mountain resembles those in the deep (Mac Tung and Scheelite Dome) and shallow (Mike Lake) reduced intrusion-related deposits in the Yukon Territory of Canada (Baker and Lang, 2001). The formation temperatures reported for these and many other reduced intrusion-related gold deposits range from 620° to 215°C (Thompson and Newberry, 2000). The phase ratios of fluid inclusions in quartz (Fig. 16) from various positions in the

system are consistent with this range of formation temperatures, especially the lower part of this range. In comparison to Carlin-type deposits (Hofstra and Cline, 2000), the fluid inclusion types at the deep level have higher gas contents and greater inferred trapping pressures, whereas the hypersaline and vapor inclusions at the shallow level are interpreted to indicate boiling, which is absent in Carlin-type deposits.

Isotopic Studies

In the following sections, lead, hydrogen, oxygen, and sulfur isotope data on ore-related minerals are used to identify the source of ore fluid components in the deep and shallow deposits. The lead isotope data in Table 4 are reproduced here from Nutt et al. (2000). Although oxygen and sulfur isotope plots were published in Nutt et al. (2000), the stable isotope data provided in Tables 5 and 7 are new. The hydrogen and oxygen isotope data on hydrous minerals and fluid inclusions in Table 6 were generated for this paper.

Pb isotopes

The Pb isotope compositions of stage 2 coarse pyrite from the shallow RBM deposit and stibnite from the peripheral LJ Ridge deposit were compared to that of a potassium-feldspar phenocryst from, and whole-rock analysis of, the Bald Mountain pluton (Table 4, reproduced from Nutt et al., 2000) but is repeated here for its importance in interpretation. The Pb isotope composition of RBM pyrite is nearly identical to that of the pluton and is only slightly different from that of stibnite from the LJ Ridge deposit. The similarity among Pb isotope compositions indicates that all or most of the Pb in the ores was derived from the Bald Mountain pluton and associated porphyritic intrusions.

Oxygen isotopes of vein quartz and jasperoid

Strata-bound jasperoids that predate the Jurassic intrusions and milky quartz veins have low $\delta^{18}O$ values (–0.8 to +6.9‰). The $\delta^{18}O$ values of vein quartz and discordant jasperoid are much higher (Table 5). The $\delta^{18}O$ value of quartz from a stage 1 milky quartz vein in the RBM deposit (13.0‰) is similar to that of quartz from milky quartz veins at Top and Sage Flat (12.0–14.2‰). Discordant jasperoid and drusy quartz veinlets within the discordant jasperoid have a wider range of $\delta^{18}O$ values (8.9–19.6‰) but with average values similar to those of milky quartz veins. Jasperoid along the trace of the Ruby fault has $\delta^{18}O$ values of 5.7 to 6.3 per mil.

In the absence of precise paleothermometric data, plausible formation temperatures must be assumed to use measured mineral isotopic compositions and the corresponding temperature dependent fractionation factors (Table 6) to calculate the isotopic composition of the fluids. If we use the full 620° to 215°C temperature range for reduced intrusion-related gold deposits cited above, the $\delta^{18}O_{H_2O}$ values calculated for milky quartz from the Top, Sage Flat, and RBM deposits extend from –0.7 to +12.2 per mil, encompassing the established range for magmatic water (5.5–9.0‰). Conversely, if we assume that the fluids were comprised of magmatic water, the quartz $\delta^{18}O$ values can be used to calculate temperatures. The $\delta^{18}O$ values for milky quartz from Top, Sage Flat, and RBM are consistent with deposition from magmatic water at temperatures between 315° and 360°C, or a mixture of magmatic and meteoric water at lower temperatures, such as 250°C (Fig. 17, Table 6). Because the wide range in $\delta^{18}O$ values for discordant jasperoid and drusy quartz veinlets are broadly similar to those of quartz from milky quartz veins, we infer that the jasperoid and drusy quartz veinlets also were deposited from magmatic fluids; the higher values reflect isotopic exchange with sedimentary rocks and the lower values mixing with meteoric water.

The strata-bound jasperoid that predates the Bald Mountain intrusive rocks and milky quartz veins and the postore jasperoid along the Ruby fault have noticeably different isotopic compositions and formed from distinctly different fluids. The low $\delta^{18}O$ values of postore jasperoid along the Ruby fault suggest it formed from meteoric water.

Oxygen and hydrogen isotopes of hydrous minerals and fluid inclusions

The $\delta^{18}O$ and δD values of fluid inclusions in milky quartz veins, milky quartz, sericite, and fluids in equilibrium with milky quartz and sericite at the above mentioned temperatures of 360° to 250°C are plotted in Figure 17, based on data in Table 6. The $\delta^{18}O$ and δD values of 1A-kaolinite and corresponding fluid compositions calculated using a temperature of 25°C also are plotted relative to traditional references.

Hydrothermal fluids in equilibrium with sericite from the Top deposit in the deeper part of the system plot within and above the magmatic water box (Fig. 17). The data points above the magmatic water box may reflect contact metamorphic water or mixing between magmatic water and exchanged meteoric water. Hydrothermal fluids in equilibrium with milky quartz veins at deep and shallow levels in the system plot within and to the left of the magmatic water box (Fig. 17), which suggests that ore fluids mixed with meteoric water.

Fluid inclusions in milky quartz veins have δD_{H_2O} values that are much lower than Late Jurassic meteoric water but within the range of Tertiary meteoric water (Fig. 17). Therefore, we infer that fluid inclusions in milky quartz veins are largely secondary in origin, Tertiary in age, and not representative of the Jurassic hydrothermal system.

TABLE 4. Pb Isotope Compositions of Samples from Bald Mountain (reproduced from Nutt et al., 2000)

	Sample no.	Mineral	$^{206}Pb/^{204}Pb$	±	$^{207}Pb/^{204}Pb$	±	$^{208}Pb/^{204}Pb$	±
Bald Mountain pluton	97-BM-16	K-feldspar	19.511	0.012	15.730	0.014	39.191	0.048
LJ deposit	LJR-STIB	Stibnite	19.843	0.014	15.763	0.015	39.005	0.049
RBM deposit	97-BM2	Pyrite	19.470	0.012	15.737	0.014	39.188	0.047

Analyses by D.M. Unruh, U.S. Geological Survey, Denver, CO, using methods similar to those described in Unruh (2002)

TABLE 5. Range of Oxygen Isotope Values of Samples from Bald Mountain (quartz, Jasperoid, and barite samples collected in this study)

	$\delta^{18}O$ (‰) range
Milky quartz vein at Top and Sage Flat	12.0 to 14.2
Milky quartz vein at RBM	13.0
Discordant Jasperoid and drusy quartz veinlets in the Jasperoid	8.9 to 19.6
Strata-bound Jasperoid at contact	–0.8 to +6.9
Brecciated Jasperoid along Ruby Mountain fault zone	5.7 to 6.3

Sample no.	Deposit/location	Host rock		Mineral or rock	$\delta^{18}O$ (‰)
Bald Mountain					
BM-99-1a	W. of Top pit	Breccia along Ruby fault		Jasp frag	5.7
BM-99-1a	W. of Top pit	Breccia along Ruby fault		Jasp matrix	6.1
BM-99-1	W. of Top pit	Breccia along Ruby fault		Jasperoid sand	6.3
BM-99-4	E. of Top pit	Pilot		Jasperoid	15.9
BM-99-5	E. of Top pit	Guilmette		Jasperoid	13.6
BM-99-5	E. of Top pit	Porphyry		Jasperoid w/ qtz phenos	12.8
BM-99-5	E. of Top pit	Porphyry		Jasperoid	16.1
Sage Flat 1	Sage Flat pit	Porphyry		Milky quartz vein	14.2
Sage Flat 2	Sage Flat pit	Porphyry		Milky quartz vein	14.8
HS-00-2Kb	Horseshoe	Porphyry dike	Upper bench	Quartz phenocryst	11.7
HS-00-1Ab	Horseshoe	Porphyry dike	Mid-level	Quartz phenocryst	12.0
BM-99-8	3 pit	Geddes	Pit	Drusy	0.5
BM-99-10	NW of 3 pit	Eldorado-Geddes	Concordant	Drusy quartz	5.5
BM-99-10	NW of 3 pit	Eldorado-Geddes	Vein	Milky quartz vein	12.0
BM-99-10	NW of 3 pit	Eldorado-Geddes	Concordant	Jasperoid	3.6
BM-99-11	SW of LJ Ridge pit	Hamburg-Dunderberg	Concordant	Drusy quartz	0.0
BM-99-11	SW of LJ Ridge pit	Hamburg-Dunderberg	Concordant	Jasperoid	–0.8
BM-99-12	SW of LJ Ridge pit	Lamprophyre	Vein	Milky quartz	14.0
BM-99-13	S. of LJ Ridge pit	Dunderberg		Jasperoid	17.4
BM-99-13	S. of LJ Ridge pit	Dunderberg		Drusy	1.7
BM-99-14	LJ Ridge pit	Dunderberg	Ore	Jasperoid	17.6
BM-99-14	LJ Ridge pit	Dunderberg	Ore	Drusy quartz	18.2
BM-99-15	LJ Ridge pit	Dunderberg	Ore	Drusy quartz	19.3
BM-99-15	LJ Ridge pit	Dunderberg	Ore	Drusy quartz	19.1
BM-99-15	LJ Ridge pit	Dunderberg	Ore	Jasperoid	19.1
BM-99-16A	N. margin Top pit	Lamprophyre dike		Milky qtz vein	14.2
BM-99-16B	N. margin Top pit	Windfall/Pogonip?		Jasperoid	10.5
BM-99-16B	N. margin Top pit	Porphyry		Jasperoid	10.0
BM-99-16B	N. margin Top pit	Porphyry		Jasperoid	8.9
BM-99-17	LJ Ridge pit	Dunderberg	Ore	Jasperoid	17.9
BM-99-18	LJ Ridge pit	Dunderberg	Ore	Drusy quartz	14.9
BM-99-18	LJ Ridge pit	Dunderberg	Ore	Jasperoid	18.7
BM-99-O	RBM pit?	Porphyry		Jasperoid	10.4
LJC-9 228	LJ Ridge core	Dunderberg	Ore	Euh.qtz, vein 2	17.5
LJC-9 228	LJ Ridge core	Dunderberg	Ore	Euh.qtz, vein 1	13.9
LJC-9 228	LJ Ridge core	Dunderberg	Ore	Jasperoid	16.5
LJC-9 228	LJ Ridge core	Dunderberg	Ore	Qtz-cc veinlet	19.6
98-LJR-stib	LJ Ridge pit	Dunderberg	Ore	Jasperoid	10.5
98-LJR-stib	LJ Ridge pit	Dunderberg	Ore	Drusy quartz	19.5
98-LJR-stib	LJ Ridge pit	Dunderberg	Ore	Drusy quartz	17.7
rbmc-1 250-260	RBM	Chainman-Porphyry	Ore	Milky quartz vein	13.0
BM-99-8	3 pit	Geddes	Pit	Drusy quartz	-0.5
Mahoney-99	N. of Mahoney pit	Guilmette?		Jasperoid	18.4
BM-99-7	3 pit	Eldorado	Pit	Drusy quartz	0.6
BM-99-7	3 pit	Eldorado	Pit	Jasperoid	0.8
BM-99-7	3 pit	Eldorado	Pit	Early drusy quartz	3.5
BM-99-8	3 pit	Geddes	Pit	Concordant Jasperoid	6.9
BM-99-7	3 pit	Eldorado	Pit	Jasperoid	3.8
Mahoney-99	N. of Mahoney pit	Guilmette		Diagenetic barite in jasperoid	12.4
BM-99-16C	N. margin Top pit	Windfall/Pogonip?		Diagenetic barite in jasperoid	16.7

[1] The $\delta^{18}O$ compositions of silicates and barite were determined using bromine pentafluoride digestions as described by Clayton and Mayeda (1963) on a Finnigan MAT 252 mass spectrometer; all analyses were conducted in analytical lab at the U.S. Geological Survey in Denver, CO

TABLE 6. δD and $\delta^{18}O$ Values of Hydrous Minerals and Fluids from Bald Mountain

Sample no.	Host unit	Mineral	δD[1]	$\delta^{18}O$[2]	Low T[3] (°C)	High T[3] (°C)	Low T[4] (°C) $\delta D(H_2O)$	Low T[4] (°C) $\delta^{18}O(H_2O)$	High T[4] (°C) $\delta D(H_2O)$	High T[4] (°C) $\delta^{18}O(H_2O)$
BM-99-10	J-milky qtz vein	F.I. H_2O, qtz	–129	12.0	250	360	–129	3.04	–129	6.65
BM-99-10	J-milky qtz vein	F.I. H_2O, qtz	–121	12.0	250	360	–121	3.04	–121	6.65
BM-99-12	J-milky qtz vein	F.I. H_2O, qtz	–138	14.0	250	360	–138	5.04	–138	8.65
Sage Flat qtz#1	J-milky qtz vein	F.I. H_2O, qtz	–153	14.2	250	360	–153	5.24	–153	8.85
Sage Flat qtz#2	J-milky qtz vein	F.I. H_2O, qtz	–153	14.8	250	360	–153	5.84	–153	9.45
Top sericite	J-qtz porphyry pluton	Sericite	–57	12.3	250	360	-40	7.3	-43	8.8
Top white sericite	J-qtz porphyry pluton	Sericite	–46	12.3	250	360	-29	7.3	-32	8.8
rbmc-2-233'	J-qtz porphyry dike	1A-kaolinite	–145	12.4	25		–116	–11.9		
rbmc-2-233'	J-qtz porphyry dike	1A-kaolinite	–146	12.4	25		–117	–11.9		
rbmc-1a-250-260	Mc	1A-kaolinite	–138	13.2	25		–108	–11.1		
rbmc-1a-250-260	Mc	1A-kaolinite	–136	13.2	25		–106	–11.1		
rbmc-1c-210-220	Mc	1A-kaolinite	–134	12.9	25		–104	–11.4		
rbmc-1c-210-220	Mc	1A-kaolinite	–129	12.9	25		–100	–11.4		
rbmc-1a-320-330vg	J-aphanitic dike (lamprophyre?)	1A-kaolinite	–139	11.9	25		–109	–12.4		
rbmc-1a-320-330vg	J-aphanitic dike (lamprophyre?)	1A-kaolinite	–141	11.9	25		–111	–12.4		
97-BM-13 (Top)	J-qtz porphyry pluton	1A-kaolinite (supergene oxidized)	–159	7.3	25		–129	–17.0		
97-BM-13 (Top)	J-qtz porphyry pluton	1A-kaolinite (supergene oxidized)	–157	7.3	25		–127	–17.0		
BM-99-14B LJ-dike	J-lamprophyre dike	1A-kaol > smectite > 3T-mica	–130	11.4	25		–100	–12.9		

Notes: Samples analyzed by W.D. Christiansen and A.H. Hofstra in R.O. Rye's laboratory at the U.S. Geological Survey in Denver, CO; abbreviations: F.I. = fluid inclusion, J = Jurassic pluton, Mc = Mississippian Chainman Formation, qtz = quartz

[1] Quartz was baked out at 75°C overnight, fluid inclusion water was extracted by crushing in stainless steel tubes and converted to H_2 using the Zn shot method and analyzed on a Finnigan MAT 252 mass spectrometer; the δD of hydrous minerals was determined using an automated thermochemical conversion elemental analyzer coupled to a Delta mass spectrometer

[2] The $\delta^{18}O$ compositions of silicates were determined using bromine pentafluoride digestions as described by Clayton and Mayeda (1963) on a Finnigan MAT 252 mass spectrometer

[3] The 250° to 360°C temperatures correspond to the quartz oxygen isotope interpretation described in the text and are within the range reported for analogous systems; the 25°C temperature is based on the interpretation described in the text that 1A-kaolinite is supergene

[4] Fractionation factors for kaolinite and Illite are from Sheppard and Gilg (1996); fractionation factor for quartz is from Zheng (1993)

TABLE 7. Range of Sulfur Isotope Values from Bald Mountain and Sulfur Isotope Values for Sulfides and Barite Collected for This Study

	δ^{34}S (‰) range
Molybdenite and chalcopyrite from Top	15.5 to 19.3
Gold-bearing pyrite and arsenopyrite from LJ Ridge	16.0 to 18.3
Late stibnite from LJ Ridge	25.4 to 26.4
Pyrite from RBM, stages 1-2	10.0 to 17.1
Botyoidal pyrite/marcasite from RBM, stage 3	–5.7 to +8
Chalcopyrite associated with gold from RBM, stage 2	10.0
Pyrite from Cambrian Secret Canyon Shale	13.3 to 17.3
Cambrian to Proterozoic siliciclastic	Average of 19.3
Barite from Ordovician Pogonip Group	29

Sample no.	Deposit/location	Host rock		Mineral	δ^{34}S[1] (‰)
BM-99-6	3 pit	Geddes	Barren	Pyrite veinlet	–3.2
BM-99-6	3 pit	Geddes	Barren	Pyrite veinlet (duplicate)	–3.1
BM-99-6	3 pit	Geddes	Barren	Pyrite dissem. cubes	–2.3
97baldmtn18	Top pit	Marble		Chalcopyrite vein	15.5
97baldmtn15	LJ haul road	Skarn	Barren	Dissem. molybdenite	17.4
97baldmtn17	Bald Mtn pluton	Pluton	Barren	Qtz-molybdenite veinlet	19.3
98-LJR-stib	LJ Ridge pit	Dunderberg	Ore	Late stibnite in jasperoid	25.4
98-LJR-stib	LJ Ridge pit	Dunderberg	Ore	Late stibnite in jasperoid	26.0
98-LJR-stib	LJ Ridge pit	Dunderberg	Ore	Late stibnite in jasperoid	26.4
ljc-1-1567	LJ Ridge core	Aplite sill	Barren	Disseminated aspy and py	22.5
bm-99-14b	LJ Ridge pit	Lamprophyre dike	Barren	Disseminated py	13.6
98-LJR-stib	LJ Ridge pit	Dunderberg	Ore	Aspy and py in jasperoid	16.0
98-LJR-stib	LJ Ridge pit	Dunderberg	Ore	Aspy and py in jasperoid	18.3
1a-320	RBM core	Aphanitic dike	Barren	Cpy w/ native gold	10.0
2-233 b	RBM core	Qtz-feldspar porphyry	Ore	Early coarse py	17.1
2-233 b	RBM core	Qtz-feldspar porphyry	Ore	Late fine-grained pyrite	11.3
1-504	RBM core	Chainman	Ore	Late py and marc	–5.7
1-210	RBM core	Chainman	Ore	Late py and marc?	–3.1
1-210	RBM core	Chainman	Ore	Late py and marc	3.5
1b-320-2	RBM core	Aphanitic dike	Ore	Late py and marc	8.0
bm-99-0	RBM pit?	Qtz-feldspar porphyry	Ore	Early and late py and marc	9.7
Mahoney-99	N. of Mahoney pit	Guilmette		Diagenetic barite in jasperoid	40.2
BM-99-16C	N. margin Top pit	Windfall/Pogonip?		Diagenetic barite in jasperoid	29.0

[1] The δ^{34}S composition of sulfide and sulfate minerals was determined by an online method, using an elemental analyzer coupled to a Micromass Optima mass spectrometer following Geiseman et al. (1994); analytical precision generally is better than ±0.2‰; all analyses were conducted in analytical lab at the USGS in Denver, CO

1A-kaolinite from deep (Top) and shallow (RBM) deposits also has low δD values and plot near the kaolinite line (Fig. 17). In comparison to hydrothermal dickite or 1M-kaolinite, the 1A-kaolinite polytype analyzed is relatively disordered, pargenetically late, and collected from weathered oxide ore at the Top deposit and from sites above or a short distance below the zone of weathering and oxidation at the RBM deposit. Based on these relationships, we infer that most of the argillic alteration in the district is supergene in origin and younger than Miocene displacement along the Ruby fault. 1A-kaolinite may have formed during the erosional event recorded by the unconformity between the Sage Flat deposit and overlying Miocene or younger volcaniclastic rocks. K-Ar dates on supergene alunite in the neighboring Alligator Ridge district (Ilchik, 1990) suggest that deep weathering and oxidation took place between 12.4 and 3.6 Ma. The δD value of supergene alunite at Alligator Ridge and 1A-kaolinite at Bald Mountain are low, suggesting they both formed during the same period of exhumation.

Sulfur isotopes

The δ^{34}S values of sulfide minerals from Bald Mountain are mostly much higher (Table 7) than those of classic porphyry Cu systems in the western United States, which normally have δ^{34}S values of 0 ± 5 per mil (Ohmoto and Rye, 1979; Ohmoto and Goldhaber, 1997). Molybdenite and chalcopyrite from the pluton and contact metamorphic aureole at the Top deposit have high δ^{34}S values (15.5–19.3‰). In the peripheral LJ Ridge deposit, δ^{34}S values of Au-bearing pyrite and arsenopyrite are also high (16.0–18.3‰). Later stage stibnite has even higher δ^{34}S values (25.4–26.4‰). In the shallow RBM deposit, stage 1–2 pyrite (10.0–17.1‰) and stage 2 chalcopyrite (10.0‰) associated with native Au and argillic alteration have δ^{34}S values that are similar to, or less than, those of molybdenite and chalcopyrite from Top. In contrast to the other sulfide minerals, the late botryoidal and dendritic pyrite and marcasite at RBM have δ^{34}S values as low as –5.7 per mil.

The δ^{34}S data suggest that much of the S in the magma was obtained from the surrounding sedimentary rocks. The δ^{34}S values of chalcopyrite and molybdenite in veinlets from the center of the system are similar to those of pyrite in the Secret Canyon Shale (13.3–17.3‰) and underlying Cambrian to Proterozoic siliciclastic sequence (avg 19.3‰: Vikre, 2000) and distinct from diagenetic disseminated pyrite and pyrite

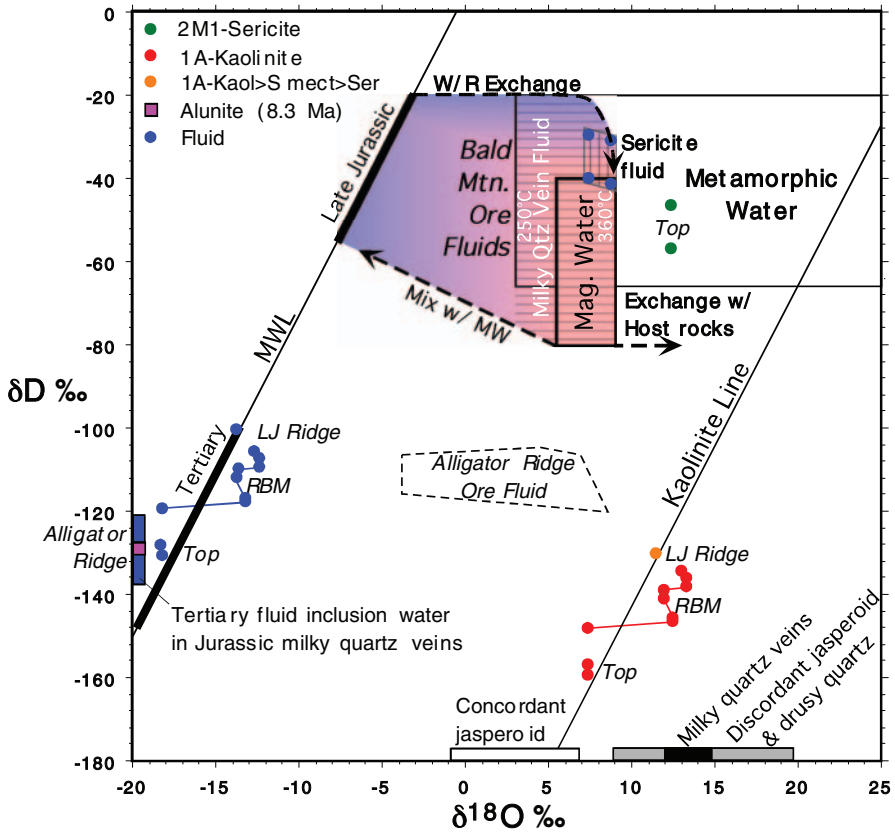

FIG. 17. Hydrogen and oxygen isotope compositions of kaolinite (red and orange circles), sericite (green circles), quartz (magenta circles), and hydrothermal fluids (blue circles) from Battle Mountain, relative to traditional references (meteoric water line, kaolinite line, and the fields for magmatic and metamorphic waters: cf. Taylor, 1979). The Tertiary and Jurassic intervals on the meteoric water line are from Hofstra et al. (1999). The Alligator Ridge ore fluid field is from Nutt and Hofstra (2003). Analytical methods, results, temperatures, and fractionation factors used are listed in Table 6. The field for the milky quartz vein fluid is based on calculated $\delta^{18}O_{H_2O}$ values, using temperatures of 250° to 360°C and the δD_{H_2O} values of magmatic water that mixed with variably exchanged Jurassic meteoric water. The field for the sericite fluid was calculated using the same temperature range.

veinlets in the Geddes Limestone (–3.2 to –2.3‰). Diagenetic barite in silicified Pogonip Group limestone also has a high $\delta^{34}S$ value (e.g., 29‰). The $\delta^{34}S$ data suggest that Bald Mountain magmas assimilated sulfur from sedimentary rocks during their ascent and/or following their emplacement. The absence of primary sulfate minerals in Bald Mountain ore deposits indicates that H_2S was the predominant sulfur species in solution, so the $\delta^{34}S_{H_2S}$ values are representative of bulk sulfur in the fluids.

The similarly high $\delta^{34}S$ values of Au-bearing pyrite and arsenopyrite (16.0–18.3‰) at the proximal LJ Ridge deposit suggest that ore fluids responsible for these minerals also were derived from the central part of the system. Late-stage stibnite from LJ Ridge has much higher $\delta^{34}S$ values (25.4–26.4‰), which indicates the nearly complete reduction of sedimentary sulfate (e.g., 29.0‰ barite) to sulfide possibly by reactions with ferrous iron minerals or organic carbon at elevated temperatures (Ohmoto and Rye, 1979).

In the shallow RBM deposit, the pyrite with higher $\delta^{34}S$ values may be derived from the intrusive center of the system, whereas the pyrite and chalcopyrite with lower values may be due to oxidation during boiling or mixing with an external source of light sulfur.

The large negative isotopic shifts in the botryoidal pyrite and marcasite may be attributed to supersaturation, a combination of cooling, oxidation, formation of metastable sulfur species, or bacterial sulfate reduction (cf. Plumlee and Rye, 1992). The late pyrite may have formed during the waning stages of the Jurassic hydrothermal system or below the oxidation front during supergene alteration. Considering that stage 3 pyrite and marcasite are restricted to the shallow level RBM deposit at a position just below the present-day zone of weathering and oxidation with 1A-kaolinite that has $\delta^{18}O$ and δD values consistent with a supergene origin, we infer that they too are supergene.

Alternative Models

Because Bald Mountain is near Mooney Basin, and particularly Alligator Ridge, which was first interpreted by Ilchik (1990) as Carlin type, the assumption has been that Bald Mountain also is Carlin type. Because reduced intrusion-related Au deposits are not recognized in northern Nevada the relationship proposed here has not been considered previously. The Bald Mountain deposits differ from the Alligator Ridge-Mooney Basin deposits in a number of ways: (1) the presence of native Au associated with Bi and base metals at

Bald Mountain contrasts with the Au in arsenian pyrite in the Mooney Basin deposits; (2) the distribution of Bald Mountain deposits around the intrusion contrasts with the distribution of the Mooney Basin deposits for 40 km along the north-striking Mooney Basin fault system; (3) much of the ore at Bald Mountain is in stockwork and concentrated along the edges of dikes and sills, whereas the ore along Mooney Basin is all disseminated; (4) ore at Bald Mountain is present in Cambrian through Mississippian rocks, whereas the ore along Mooney Basin is restricted to a thin stratigraphic section of Devonian and Mississippian rocks; and (5) deposits at Bald Mountain formed at depths of kilometers, whereas deposits along Mooney Basin formed at shallow depths of no more than 600 m (Nutt and Hofstra (2003). A comparison with the Carlin-type Casino deposit illustrates some of these differences. Both are in Mississippian Chainman Shale, but at Casino the ore is in a large jasperoid and Chainman Shale (Nutt and Hofsta, 2003), whereas the RBM deposit is hosted mostly in intrusive rock and to a lesser extent Chainman Shale and native Au is present and intergrown with base metal sulfides.

The similar Pb isotope values of the ore and pluton at Bald Mountain contrasts with Eocene Carlin-type gold deposits in the Carlin and Getchell trends where Pb is interpreted to have been derived primarily from Neoproterozoic to Devonian sedimentary rocks (Tosdal et al., 2003). The Bald Mountain Pb isotope data also are unlike those of Eocene igneous rocks in the Carlin trend, as well as Eocene igneous rocks and sulfides in the Tuscarora epithermal Au-Ag district (Castor et al., 2003), consistent with Bald Mountain being unrelated to Eocene igneous or hydrothermal activity.

Schmauder et al. (2005) proposed a Miocene age for the Bald Mountain deposits, based on a range of Miocene apatite-fission track ages and $\delta^{18}O$ values of 5 to 16 per mil obtained from the ore-hosting Bida trend. Our $\delta^{18}O$ values are similar, and it is possible that the Bida trend repeatedly focused fluid flow into the area. However, the plot of fission-track samples in Schmauder et al. (2005) shows no faults, and they state that apatite ages were not reset by uplift of the East Humboldt-Ruby Mountain core complex just north of Bald Mountain. Our mapping (Nutt and Hart, 2004) shows numerous faults, and the large-displacement Ruby fault on the west side of the range (Fig. 6) is younger than 35 Ma volcanic rocks that are in debris flows and blocks on the downthrown side of the fault. Other studies on apatite in the Ruby Mountains record uplift and cooling at about 25 to 15 Ma, about the same age range found in the Bald Mountain area (Dokka et al., 1986; K. A. Howard, U.S. Geological Survey, pers. commun., 2005). These studies suggest that the Miocene events were regional and not restricted to the Bald Mountain area. Schmauder et al. (2005) emphasized that apatite fission tracks in rocks away from the Bida trend are not reset. Many of these samples are from Devonian and Mississippian rocks. Eocene rocks rest on the Devonian and Mississippian rocks, indicating that they were exposed at about 36 Ma. Therefore, any Jurassic dikes cutting Devonian and Mississippian rocks in the footwall would not be expected to be reset during Miocene uplift.

Jasperoid from the fault zone along the haul road to the Top pit and along the Ruby fault (sample BM-99-1) where it is exposed in Bourne Canyon contains no Au, and the occurrence along the haul road has a $\delta^{18}O$ value indicating formation from meteoric water. We propose that the Miocene apatite ages are due to uplift of the Ruby Mountains and associated meteoric water circulation along both the extensional Ruby Mountain fault and intersecting Bida trend.

Conclusions

Our studies show that Au deposits in the Bald Mountain mining district are related to a Late Jurassic intrusive center. The deposits occur along or near a crustal fault zone (Bida trend) that was an open structure in the Jurassic. Jurassic intrusive rock was emplaced along this crustal fault zone and, other than dikes, is restricted to it. The fault extended to great depths, as shown by the Pb isotope data of intrusions, a magnetotelluric survey that modeled intrusive rocks to great depths, and the presence of lamprophyres. A crustal component is apparent in the Sr and O values (Table 5, 11.7–12.0‰ of quartz phenocrysts from a Bald Mountain porphyry dike; Wooden et al., 1999; King et al., 2004). The presence of free Au, Bi sulfide minerals, and the association of Au with Cu, Pb, Sb, Tl, Sn, Ni, and Fe all suggest a magmatic hydrothermal origin. In addition, hydrothermal sericite from the Top deposit is Jurassic in age and has δD values of magmatic water (Fig. 17). It is clear that meteoric fluids from the neighboring Eocene Alligator Ridge hydrothermal system entered the Bida trend at its intersection with the Mooney Basin fault zone to form the Horseshoe Carlin-type Au deposit (Nutt and Hofstra, 2003). Although Eocene (~52–34 Ma) apatite fission track dates on rocks in the Bida trend (Schmauder et al., 2005) suggest that hydrothermal fluids were discharged along it to the northwest, we found little or no mineralogical or geochemical evidence that they deposited much Au. Furthermore, on the west side of the Miocene Ruby fault, where Paleozoic sedimentary rocks, Jurassic intrusive rocks, and Tertiary sedimentary and volcanic rocks occur in slide blocks, only Paleozoic rocks cut by intrusive rocks are mineralized.

The Bald Mountain pluton and associated Au deposits are similar in most respects to reduced intrusion-related Au deposits (McCoy et al., 1997; Thompson et al., 1999; Lang et al., 2000; Thompson and Newberry, 2000) but are distinct from Eocene Carlin-type deposits (Tables 8, 9). In particular, the Bald Mountain deposits have a variety of Bi minerals and Bi enrichment and Au in quartz veins.

A number of factors somewhat unique to deposits in the Bald Mountain area lead us to propose the following model for the district. The district is in a back-arc setting near a northwest-striking crustal fault zone (southern extension of the Carlin trend) inherited from Precambrian rifting. Jurassic deformation opened a northwest-striking crustal feature along the Bida trend, facilitating ascent and emplacement of both felsic magmas derived from a deeper crustal and/or subcontinental magma reservoir and lamprophyre magmas derived from a mantle source. Compositional zoning in magnetite from a dike suggests that magma mixing or assimilation may also be important (Fig. 7C). Felsic magmas appear to have evolved from a normal oxidized state to a substantially more reduced state by assimilation of calcareous carbonaceous and pyritic country rocks such that ilmenite became stable during the later evolutionary stages of the system. Assimilation of country rocks caused the magma to cool, and

TABLE 8. Characteristics that Distinguish Late Jurassic Intrusion-Related and Late Eocene Carlin-Type Gold Deposits in the Bald Mountain-Alligator Ridge Area[1]

Bald Mountain: Intrusion-related gold deposits	Alligator Ridge-Mooney Basin: Carlin-type gold deposits
Deposits concentrically distributed around Jurassic intrusion	Deposits distributed for 40 km along north to northeast trend
The largest deposit (Top/Mahoney, active) has produced ca. 500,000 oz of Au at a grade of 2 g/t, reserves of >500,000 oz	The largest deposit (Alligator Ridge, inactive) produced 787,500 oz of Au at 4 g/t
Emplacement of pluton along dilatant NW faults	Dilation of northerly faults consistent with late Eocene northwest-southeast extension
Ore in Cambrian to Mississippian rocks; primarily in Cambrian-Ordovician rocks and Jurassic intrusions; vertical extent 3,000 m, lateral extent <2,500 m from pluton	Ore restricted to Devonian and Mississippian rocks, and primarily to an interval less than 50 m thick in the Pilot Shale
Alteration types, ore minerals, textures, and coupled introduction of base metals, Fe, S, and Au similar to other intrusion-related gold deposits	Alteration types, ore minerals, and coupled introduction of S and Au without base metals typical of Carlin-type gold deposits
Coarse native gold associated with chalcopyrite and Bi sulfides; native gold in milky quartz veins; invisible gold in crystalline arsenopyrite and As pyrite	Invisible gold in poorly crystalline As pyrite and marcasite; no milky quartz veins or native gold
Zoned geochemical bullseye around pluton; variable enrichments of Au, Ag, W, Sn, Mo, Cu, Pb, Zn, Bi, Te, Sb, As, Hg	No geochemical zoning relative to pluton; enrichment of Au, As, Sb, Hg, Tl
Pb isotopes of intrusion and ore are similar	No data; Pb isotopes of arsenian pyrite in other districts are similar to host strata or underlying Neoproterozoic siliciclastic rocks (Tosdal et al., 2003)
Stable isotopes: magmatic fluids evolve by reactions with country rock and mixing with local ground water; sulfur from assimilation of sedimentary rocks	Stable isotopes: exchanged meteoric water, sulfur from sedimentary rocks, similar $\delta^{18}O$ of ore-grade jasperoid and Eocene jasperoid
Fluid inclusions: hot, deep, boiling at RBM	Fluid inclusions: warm, shallow
Bald Mountain pluton, dikes, and hydrothermal sericite are similar in age	Late Eocene volcanic rocks are younger than gold deposits; jasperoid younger than Eocene sedimentary rocks

[1] Data for Bald Mountain are from this study; data for Alligator Ridge are from Nutt and Hofstra (2003) and Ilchik (1990)

TABLE 9. Comparison between Reduced Intrusion-Related Gold Deposits and Bald Mountain Deposits [1]

Reduced intrusion-related gold	Bald Mountain
Intrusion most common in thick siliciclastic continental margin sequences, in places carbonaceous, overlying older continental crust, or metamorphosed equivalent	Intrusion in Proterozoic to Cambrian sedimentary marine sequences which are in places carbonaceous, near boundary between Proterozoic and Archean basement
Metaluminous, subalkalic intrusions of intermediate to felsic composition, mostly granodiorite to granite	Metaluminous, subalkalic, quartz monzonite, minor granodiorite, aplite, lamprophyre
Span the boundary between ilmenite and magnetite series	Scarce ilmenite and rare magnetite, see discussion of Fe-Ti oxides
Low magnetic susceptibilities reflected in weak to absent magnetic highs in aeromagnetic data	No magnetic signature
Initial $^{87}Sr/^{86}Sr$ ratios from 0.709 to 0.720	Initial $^{87}Sr/^{86}Sr$ ratio of 0.7104
Accessory phases are zircon, monazite, apatite, allanite, and thorite	Accessory phases are zircon, monazite, apatite, allanite, and thorite
Gold preciptitated early at high temperatures and later at lower temperatures	Gold deposited in early milky quartz veins; late gold in RBM mineralization
Formed at depths of >5 km to near surface	Formed at depths of <6 to 3.1 km
Geochemical signature: near intrusion Au, Bi, Te, W, As, Mo; peripheral Au, As, Sb, ±Hg or base metals	Geochemical signature: near intrusion Au, Bi, Cu, Te, W, As, Mo; peripheral Au, As, Sb, ±Hg or base metals
Sulfur isotopes typically 0 ± 5‰ (magmatic), but at least one exception with sulfur derived from wall rock	Sulfur isotopes ~17–19.3‰ (sulfur derived from country rock)
$^{206}Pb/^{204}Pb$ = 19.00–19.45, $^{207}Pb/^{204}$ = 15.58–15.57; same as pluton feldspar (in interior Alaska province)	$^{206}Pb/^{204}Pb$ = 19.46–19.86, $^{207}Pb/^{204}$ = 15.72–15.78; same as pluton feldspar
In provinces generally known for W ± Sn, Mo, Bi	In gold province, southern extension of Carlin Trend, and only recognized deposit of its type; area explored for W, Cu
Sulfide poor, pyrite, arsenopyrite most abundant	Sulfide poor, pyrite, arsenopyrite, chalcopyrite, Bi-minerals, late marcasite
Carbon dioxide abundant in fluid inclusions in hydrothermal veins	Carbon dioxide in fluid inclusions

[1] Data for Bald Mountain deposits from this study; data for intrusion-related gold deposits from McCoy et al. (1997), Thompson et al. (1999), Lang et al. (2000), Thompson and Newberry (2000), Lang and Baker (2001)

volatile components (mainly CO_2 and H_2S) and possibly some metals were added. Aqueous fluids exsolved from the magma were enriched in CO_2 and H_2S but lacked significant oxidized sulfur species (SO_2 and SO). In the reduced H_2S-rich fluids, solubilities of Cu and other base metals were lower (Heinrich, 2005) and the solubility of Au higher (Loucks and Mavrogenes, 1999) than those of oxidized fluids in classic porphyry copper systems. As ore fluids emanating from the Jurassic intrusion moved into surrounding rocks and crossed steep temperature, pressure, and chemical gradients, ore deposits formed with characteristics that define a classic magmatic hydrothermal mineral and geochemical zonation pattern, but with smaller amounts of Cu and base metals and a larger proportion of Au than in typical porphyry copper systems. At deeper levels, Au precipitated with base metal sulfide and sulfosalt minerals, quartz, sericite, and carbonate minerals from episodically immiscible aqueous and carbonic fluids. At shallower levels, Au precipitated with base metal sulfide and sulfosalt minerals, quartz, and sericite during boiling that produced hypersaline brine and vapor that likely condensed at shallower, unpreserved levels in the system. Subsequent Neogene exhumation, deep weathering, and oxidation of low-grade sulfide ore was of critical importance because it made the deposits economic to mine and process using cyanide heap-leach methods.

Acknowledgments

We thank Placer Dome, N.A., Inc. for access to the deposits and core. Stimulating discussions with their geologists allowed a variety of ideas to be tested and improved our work. Jim Brandy and Kerry Hart were particularly helpful in directing our sampling and in discussing data. We thank Bill Christiansen and Cyndi Kester for isotopic analyses, Ian Ridley for LA-ICP-MS analyses, Poul Emsbo for electron microprobe analyses, and Steve Sutley for XRD analyses. The paper benefited from reviews by E.A. du Bray and J.R. Lang. Reviews by Steve Garwin and Mark Hannington substantially improved the manuscript.

September 21, 2005; October 10, 2007

REFERENCES

Ague, J.J., and Brimhall, GH., 1988a, Magmatic arc asymmetry and distribution of anomalous plutonic belts in the batholiths of California: Effects of assimilation, crustal thickness, and depth of crystallization: Geological Society of America Bulletin, v. 100, p. 912–927.

——1988b, Regional variations in bulk chemistry, mineralogy, and the compositions of mafic and accessory minerals in the batholiths of California: Geological Society of America Bulletin, v. 100, p. 891–911.

Atkinson, W.W., Jr., Kaczmarowski, J.H., and Erickson, A.J., Jr., 1982, Geology of a skarn-breccia orebody at the Victoria mine, Elko County, Nevada: Economic Geology, v. 77, p. 899–918.

Babcock, R.C., Jr., Ballantyne, G.H., and Phillips, C.H., 1995, Summary of the geology of the Bingham district, Utah: Arizona Geological Society Digest, v. 20, p. 316–335.

Baker, T., and Lang, J.R., 2001, Fluid inclusion characteristics of intrusion-related gold mineralization, Tombstone tungsten magmatic belt, Yukon Territory, Canada: Mineralium Deposita, v. 36, p. 563–582.

Blake, J.W., 1964, Geology of the Bald Mountain intrusive, Ruby Mountains, Nevada: Brigham Young University Geology Studies, v. 11, p. 3–35.

Bodnar, R.J., 1995, Fluid inclusion evidence for a magmatic source for metals in porphyry copper deposits: Mineralogical Association of Canada Short Course, v. 23, p. 139–150.

Bodnar, R.J., Reynolds, T.J., and Kuehn, C.A., 1985, Fluid inclusion systematics in epithermal systems: Reviews in Economic Geology, v. 2, p. 74–98.

Bucher, K., and Frey, M., 1994, Petrogenesis of metamorphic rocks: Berlin, Federal Republic of Germany (DEU), Springer-Verlag, 318 p.

Castor, S.B., Boden, D.R., Henry, C.D., Cline, J.S., Hofstra, A.H., McIntosh,W.C., Tosdal, R.M., and Wooden, J.P., 2003, Geology of the Eocene Tuscarora volcanic-hosted epithermal precious metal district, Elko county, Nevada: Economic Geology v. 98, p. 339–366.

Clark, D.A., 1999, Magnetic petrology of igneous intrusions: Implications for exploration and magnetic interpretation: Exploration Geophysics, v. 30, p. 5–26.

Clayton, R.N., and Mayeda, T.K., 1963, The use of bromine pentafluoride in the extraction of oxygen from oxides and silicates for isotopic analysis: Geochimica et Cosmochimica Acta, v. 27, p. 43–52.

Cline, J.S., Hofstra, A.H., Muntean, J.L., Tosdal, R.M., and Hickey, K.A., 2005, Carlin-type gold deposits in Nevada, USA: Essential features, viable models, and comparisons to similar dposits: Economic Geology 100th Anniversary Volume, p. 451–484.

Cox, D.P., 1986, Descriptive model of polymetallic veins: U.S. Geological Survey Bulletin 1693, p. 125.

Dilles, J.H.,and Proffett, J.M., 2000, Metallogenesis of the Yerington btholith, Nevada: Society of Economic Geologists Guidebook Series, v. 32, p. 45–54.

Dilles, J.H., Einaudi, M.T., Proffett, J., and Barton, M.D., 2000, Overview of the Yerington porphyry copper district: Magmatic to nonmagmatic sources of hydrothermal fluids: Their flow paths and alteration effects on rocks and Cu-Mo-Au ores: Society of Economic Geologists Guidebook Series, v. 32, p. 55–66.

Dokka, R.K., Mahaffie, M.J., and Snoke, A.W., 1986, Thermochronologic evidence of major tectonic denudation associated with detachment faulting, northern Ruby Mountains-East Humboldt Range, Nevada: Tectonics, v. 5, p. 995–1006.

Elison, M.W., 1995, Causes and consequences of Jurassic magmatism in the northern Great Basin: Implications for tectonic development: Geological Society of America Special Paper 299, p. 249–265.

Emsbo, P., Hofstra, A.H., and Luaha, E.A., 2000, Jurassic auriferous polymetallic mineralization at the Goldstrike mine, Carlin Trend, Nevada [abs.]: Geology and Ore Deposits 2000: The Great Basin and Beyond Symposium, Geological Society of Nevada, Reno/Sparks, Nevada, May 2000, Proceedings, p. B2.

Feenstra, A., and Peters, T., 1996, Experimental determinations of activities in $FeTiO_3$-$MnTiO_3$ ilmenite solid solution by redox reversals: Contributionsto Mineralogy and Petrology, v. 126, p. 109–120.

Frost, B.R., and Lindsley, D.H., 1991, Occurrence of iron-titanium oxides in igneous rocks: Reviews in Mineralogy, v. 25, p. 433–468.

Giesemann, A., Jager, H.J., Norman, A.L., Krouse, H.R., and Brand, W.A., 1994, On-line sulfur isotope determination using elemental analyzer coupled to a mass spectrometer: Analytical Chemistry, v. 66, p. 2,816–2,819.

Hedenquist, J.W., Arribas, A., Jr., and Reynolds, T.J., 1998, Evolution of an intrusion-centered hydrothermal system: Far Southeast-Lepanto porphyry-epithermal Cu-Au deposits: Economic Geology, v. 93, p. 373–404.

Heinrich, C.A., 2005, The physical and chemical evolution of low-salinity magmatic fluids at the porphyry to epithermal transition: a thermodynamic study: Mineralium Deposita, v. 39, p. 864–889.

Heitt, D.G., Dunbar, W.W., Thompson, T.B., and Jackson, R.G., 2003, Geology and geochemistry of the Deep Star gold deposit, Carlin Trend, Nevada: Economic Geology, v. 98, p. 1,107–1,135.

Henry, C.D., and Boden, D.R., 1998, Eocene magmatism: the heat source for Carlin-type gold deposits of northern Nevada: Geology, v. 26, p. 1,067–1,070.

Hitchborn, A.D., Arbonies, D.G., Peters, S.G., Connors, K.A., Noble, D.C., Larson, L.T., Beebe, J.S., and McKee, E.H., 1996, Geology and gold deposits of the Bald Mountain mining district, with Pine County, Nevada: Geology and Ore Deposits of the American Cordillera Symposium, Geological Society of Nevada, Reno, Nevada, Proceedings, p. 505–546.

Hofstra, A.H., and Cline, J.S., 2000, Characteristics and models for Carlin-type gold deposits: Reviews in Economic Geology, v. 13, p. 163–220.

Hofstra, A.H., Snee, L.W., Rye, R.O., Folger, H.W., Phinisey, J.D., Loranger, R.J., Dahl, A.R., Naeser, C.W., Stein, H.J., and Lewchuk, M., 1999, Age constraints on Jerritt Canyon and other Carlin-type gold deposits in the western United States: Relationship to mid-Tertiary extension and magmatism: Economic Geology, v. 94, p. 769–802.

Hose, R.K., and Blake, M.C., Jr., 1976, Geology and mineral resources of White Pine County, Nevada. Part I. Geology: Nevada Bureau of Mines and Geology Bulletin 85, p. 1–35.

Ilchik, R.P., 1990, Geology and geochemistry of the Vantage gold deposits, Alligator Ridge-Bald Mountain mining district, Nevada: Economic Geology, v. 85, p. 50–75.

John, D.A., Hofstra, A.H., and Theodore, T.G., 2003, A special issue devoted to gold deposits in northern Nevada: Part 1. Regional studies and epithermal deposits: Economic Geology, v. 98, p. 225–234.

Johnson, E.A., Dubiel, R.F., Litwin, R.J., Brouwers, E.M., Ash, S.R., and Good, S.C., 1993, Triassic and Jurassic rocks at Currie, Nevada? Preliminary paleontologic evidence [abs.]: Geological Society of America Program with Abstracts, v. 25, no. 5, p. 57–58.

King, E.M., Valley, J.W., Plutonli, D.F., and Wright, J.E., 2004, Oxygen isotope trends of granitic magmatism in the Great Basin: Location of the Precambrian craton boundary as reflected in zircons: Geological Society of America Bulletin, v. 116, p. 451–462.

Lang, J.R., and Baker, T., 2001, eds., Intrusion-related gold systems: Mineralium Deposita v. 36, p.477–621.

Lang, J.R., Baker, T., Hart, C.J.R., and Mortensen, J.K., 2000, An exploration model for intrusion-related gold systems: Society of Economic Geologists Newsletter, v. 40, no. 1, p. 7–15.

Loucks, R.R. and Mavrogenes, J.A., 1999, Gold solubility in supercritical hydrothermal brines measured in synthetic fluid inclusions: Science, v. 284, p. 2,159–2,163.

Lucas, S.G., and Goodspeed, T.H., 1993, The Triassic section north of Currie, Elko County, Nevada [abs.]: Geological Society of America Program with Abstracts, v. 25, no. 5, p. 111.

McCoy, D.T., Newberry, R.J., Layer, P.W., DiMarchi, J.J., Bakke, A., Masterman, J.S., and Minehane, D.L., 1997, Plutonic related gold deposits of interior Alaska: Economic Geology Monograph 9, p. 151–190.

McDougall, I., and Harrison, T.M., 1988, Geochronology and thermochronology by the $^{40}Ar/^{39}Ar$ method: Oxford Monographs on Geology and Geophysics 7, 212 p..

Miller, D.M., and Hoisch, T.D., 1995, Jurassic tectonics of northeastern Nevada and northwestern Utah from the perspective of barometric studies: Geological Society of America Special Paper 299, p. 267–294.

Mortensen, J.K., Thompson, J.F.H., and Tosdal, R.M., 2000, U-Pb age constraints on magmatism and mineralization in the northern Great Basin: Geology and Ore Deposits 2000: The Great Basin and Beyond Symposium, Geological Society of Nevada, Reno/Sparks, Nevada, May 2000, Proceedings, p. 419–438.

Nolan, T.B., 1962, The Eureka mining district, Nevada: U.S. Geological Survey Professional Paper 406, 78 p.

Nutt, C.J., 2000, Geologic map of the Alligator Ridge area, including the Buck Mountain East and Mooney Basin Summit quadrangles and parts of the Sunshine Well NE and Long Valley Slough quadrangles, White Pine County, Nevada: U.S. Geological Survey Map I–2691, scale 1:24,000.

Nutt, C.J., and Good, S.C., 1998, Recognition and significance of Eocene deformation in the Alligator Ridge area, central Nevada: U.S. Geological Survey Open-File Report 98–338, p. 141–150.

Nutt, C.J., and Hart, K.S., 2004, Geologic map of the Big Bald Mountain Quadrangle and part of the Tognini Spring Quadrangle: Nevada Bureau of Mines and Geology Map 145, scale 1: 24,000, 9 p.

Nutt, C.J., and Hofstra, A.H., 2003, Alligator Ridge district, east-central Nevada: Carlin-type gold mineralization at shallow depths: Economic Geology, v. 98, p. 1,225–1,241.

Nutt, C.J., Hofstra, A.H., Hart, K.S., and Mortensen, J.K., 2000, Structural setting and genesis of gold deposits in the Bald Mountain-Alligator Ridge area, east-central Nevada: Geology and Ore Deposits 2000: The Great Basin and Beyond Symposium, Geological Society of Nevada, Reno/Sparks, Nevada, May 2000, Proceedings, p. 513–537.

Ohmoto, H. and Goldhaber, M.B., 1997, Sulfur and carbon isotopes, *in* Barnes, H.L., ed., Geochemistry of hydrothermal ore deposits, 3rd ed.: New York, John Wiley and Sons, p. 517–612.

Ohmoto, H., and Rye, R.O., 1979, Isotopes of sulfur and carbon, *in* Barnes, H.L., ed., Geochemistry of hydrothermal ore deposits, 2nd ed.: New York, John Wiley and Sons, p. 509–567.

Plumlee, G.S. and Rye, R.O., 1992, Mineralogic, isotopic, and other characteristics of the fringes of diverse hydrothermal systems: The perithermal environment [abs.]: V.M. Goldschmidt Conference, 3rd, Reston, Virginia, May 2-9, 1992, Proceedings.

Ponce, D.A., 1991, Gravity and magnetic anomalies in the Ely quadrangle, Nevada, and anomalies related to granitic plutons: Geology and Ore Deposits of the Great Basin Symposium, Geological Society of Nevada, Reno/Sparks, Nevada, April 1991, Proceedings, p. 103–106.

Ressel, M.S., and Henry, C.D., 2006, Igneous geology of the Carlin Trend, Nevada: Development of the Eocene plutonic complex and significance for Carlin-type gold deposits: Economic Geology, v. 101, p. 347–283.

Ridley, W.I., 2000, The ICP-MS laser microprobe: A new geochemical tool: Trends in Geochemistry, v. 1, p. 1–14.

Rigby, J.K., 1960, Geology of the Buck Mountain-Bald Mountain area, southern Ruby Mountains, White Pine County, Nevada, *in* Boettcher, J.W., and Sloan, W.W., Jr., eds., Guidebook to the geology of east-central Nevada: Intermountain Association of Petroleum Geologists and Eastern Nevada Geological Society Annual Field Conference, 11th, 1960, Salt Lake City, Utah, p. 173–180.

Rodriguez, B.D. and Williams J.M., 2001, Deep regional resistivity structure across the Battle Mountain-Eureka and Carlin trends, north-central Nevada: U. S. Geological Survey Open-File Report 01-346, 165 p.

Roedder, E., 1984, Fluid inclusions: Reviews in Mineralogy, v. 12, 644 p.

Rusk, B.G., Reed, M.H., Dilles, J. H., Klemm, L.M., and Heinrich, C.A., 2004, Compositions of magmatic hydrothermal fluids determined by LA-ICP-MS of fluid inclusions from the porphyry copper-molybdenum deposit at Butte, MT: Chemical Geology, v. 210, p. 173–199.

Schmauder, G.C., Arehart, G.B., and Donelick, R., 2005, Thermal and chemical profiling of gold deposits in the Bald Mountain district, White Pine County, Nevada, *in* Rhoden, H.N., Steininger, R.C., and Vikre, P.G., eds., Window to the World: Reno, Nevada, Geological Society of Nevada, p. 531–542.

Shawe, D.R., 1977, Continent-margin tectonics and ore deposits, western United States: Transactions of the American Institute of Mining, Metallurgical and Petroleum Engineers (AIME), v. 262, p. 185–190.

Sheppard, S.M.F. and Gilg, H.A., 1996, Stable isotope geochemistry of clay minerals: Clay Minerals, v. 31, p. 1–24.

Sillitoe, R.H., 1997, Characteristics and controls of the largest porphyry copper-gold and epithermal gold deposits in the circum-Pacific region: Australian Journal of Earth Sciences v. 44, p. 373–388.

Stewart, J.H., and McKee, E.H., 1977, Geology and mineral deposits of Lander County, Nevada: Nevada Bureau of Mines and Geology Bulletin 88, 106 p.

Taylor, H.P., 1979, Oxygen and hydrogen isotope relationships in hydrothermal mineral deposits, *in* Barnes, H.L., ed., Geochemistry of hydrothermal ore deposits, 2nd ed.: New York, John Wiley and Sons, p. 236–277.

Theodore, T.G., 2000, Geology of pluton related mineralization at Battle Mountain, Nevada: Monographs in Mineral Resource Science 2, 271 p.

Thompson, J.F.H., and Newberry, R.J., 2000, Gold deposits related to reduced granitic intrusions: Reviews in Economic Geology, v. 13, p. 377–400.

Thompson, J.F.H., Sillitoe, R.H., Baker, T., Land, J.R., and Mortensen, J.K., 1999, Intrusion-related gold deposits associated with tungsten-tin provinces: Mineralium Deposits, v. 34, p. 323–334.

Thorman, C.H., Ketner, K.B., Brooks, W.E., Snee, L.W., and Zimmermann, R.A., 1991, Late Mesozoic-Cenozoic tectonics in northeastern Nevada: Geology and Ore Deposits of the Great Basin Symposium, Geological Society of Nevada Symposium, Reno/Sparks, Nevada, April 1991, Proceedings, p. 25–45.

Tosdal, R.M., Wooden, J.L., and Kistler, R.W., 2000, Geometry of the Neoproterozoic continental break-up and implications for location of Nevadan mineral belts: Geology and Ore Deposits 2000: The Great Basin and Beyond Symposium, Geological Society of Nevada, Reno/Sparks, Nevada, May 2000, Proceedings, p. 451–466.

Tosdal, R.M., Cline, J.S., Fanning, C.M., and Wooden, J.L., 2003, Lead in the Getchell-Turquoise Ridge Carlin-type gold deposits from the perspective of potential igneous and sedimentary rocks sources in northern Nevada: Implications for fluid and metal sources: Economic Geology, v. 98, p. 1,189–1,211.

Unruh, D.M., 2002, Lead isotopic analyses of selected soil samples from the USEPA Vasquez Blvd.-I-70 study area, Denver, CO: U.S. Geological Survey Open-File Report OF 02-0321, 57 p.

Vikre, P.G., 2000, Subjacent crustal sources of sulfur and lead in eastern Great Basin metal deposits: Geological Society of America Bulletin v. 112, p. 764–782.

Wannamaker, P.E., and Doerner, W.M., 2002, Crustal structure of the Ruby Mountains and southern Carlin Trend region, Nevada, from magnetotelluric data: Ore Geology Reviews, v. 21, p. 185–210.

Ward, P.L, 1995, Subduction cycles under western North America during the Mesozoic and Cenozoic eras: Geological Society of America Special Paper 299, p. 1–45.

Westra, G., 1979, Porphyry-copper genesis at Ely, Nevada: Nevada Bureau of Mines and Geology Report 33, p. 127–139.

Wooden, J.L., Kistler, R.W., and Tosdal, R.M., 1999, Strontium, lead, and oxygen isotopic data for granitoid and volcanic rocks from the northern Great basin and Sierra Nevada, California, Nevada and Utah: U.S. Geological Survey Open-File Report 99–569, 20 p.

Wright, J.E., and Wooden, J.L., 1991, New Sr, Nd, and Pb isotopic data from plutons in the northern Great Basin: Implications for crustal structure and granite petrogenesis in the hinterland of the Sevier thrust belt: Geology, v. 19, p. 457–460.

Zamudio, J.A., and Atkinson, W.W., Jr., 1995, Mesozoic structures of the Dolly Varden Mountains and Currie Hills, Elko County, Nevada: Geological Society of America Special Paper 299, p. 295–311.

Zheng, 1993, Calculation of oxygen isotope fractionations in anhydrous silicate minerals: Geochimica et Cosmochimica Acta, v. 57, p. 1,079–1,091.